Track-based alignment

of the CMS central tracker system

Patrick L.S. Connor

(on behalf of the CMS collaboration)

Universität Hamburg

1 September 2021

Introduction

The CMS tracker

Alignment

The CMS tracker

Purpose

Reconstruct tracks from **hits in silicon modules** with $\sigma_{\text{hit}} \sim \mathcal{O}(10\ \mu\text{m})$.

The CMS tracker

Purpose

Reconstruct tracks from **hits in silicon modules** with $\sigma_{\text{hit}} \sim \mathcal{O}(10\ \mu\text{m})$.

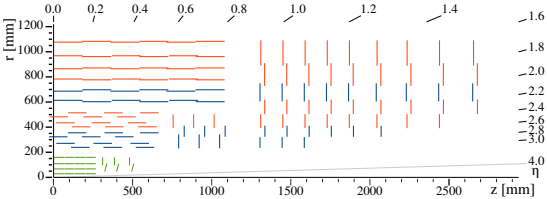

Figure from [1]

A few key figures

	subdetectors	#modules
Pixel (0)	BPIX FPIX	1440
Pixel (1)	*id.*	1852
Strip	TIB TID TOB TEC	15 148

The CMS tracker

Purpose

Reconstruct tracks from **hits in silicon modules** with $\sigma_{\text{hit}} \sim \mathcal{O}(10\ \mu\text{m})$.

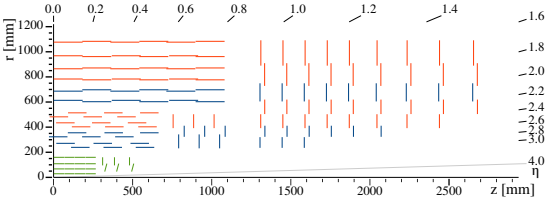

A few key figures

	subdetectors	#modules
Pixel (0)	BPIX FPIX	1440
Pixel (1)	*id.*	1852
Strip	TIB TID TOB TEC	15 148

Figure from [1]

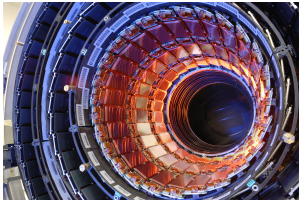

Challenges

- After mechanical alignment, $\sigma_{\text{align}} \sim \mathcal{O}(100\ \mu\text{m})$.
- Modules and substructures are moving with time.

Alignment

What you think your tracker is doing

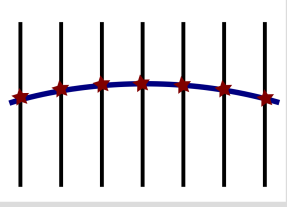

What it really looks like

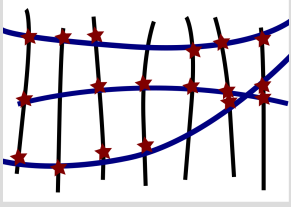

What you think your tracker is doing

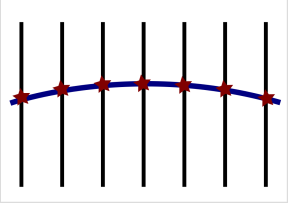

What it really looks like

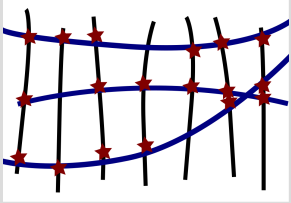

Alignment

Alignment in a nutshell

Determine the **position, orientation and surface deformation** of the $\sim 20k$ sensors of the CMS tracker (the largest silicon tracker in the world in size and in granularity), **including time variations**, during and after data taking.

What you think your tracker is doing

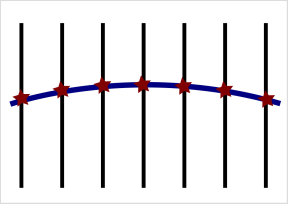

What it really looks like

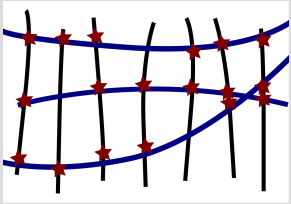

Alignment

Alignment in a nutshell

Determine the **position, orientation and surface deformation** of the $\sim 20k$ sensors of the CMS tracker (the largest silicon tracker in the world in size and in granularity), **including time variations**, during and after data taking.

Scope of this presentation

General strategies of alignment of the central silicon tracker, especially with Run-2 data.

Alignment

What you think your tracker is doing

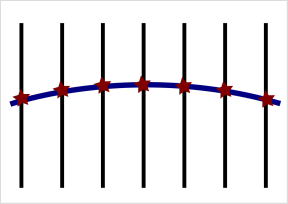

What it really looks like

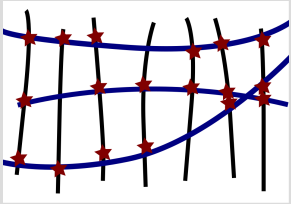

Alignment in a nutshell

Determine the **position, orientation and surface deformation** of the $\sim 20k$ sensors of the CMS tracker (the largest silicon tracker in the world in size and in granularity), **including time variations**, during and after data taking.

Scope of this presentation

General strategies of alignment of the central silicon tracker, especially with Run-2 data.

Why you should be interested in tracker alignment

Techniques are of broader interest, *e.g.* high-granularity detectors, muon chambers, etc.

General concepts

Introduction

Track-based alignment

$$\chi^2(\mathbf{p},\mathbf{q}) = \sum_j^{\text{tracks}} \sum_i^{\text{hits}} \left(\frac{m_{ij} - f_{ij}(\mathbf{p},\mathbf{q}_j)}{\sigma_{ij}} \right)^2$$

where $\mathbf{p}$ ($\mathbf{q}$) stands for the alignment (track) parameters,
and m (f) corresponds to the measurement (prediction).

Introduction

Track-based alignment

$$\chi^2(\mathbf{p},\mathbf{q}) = \sum_j^{\text{tracks}} \sum_i^{\text{hits}} \left(\frac{m_{ij} - f_{ij}(\mathbf{p},\mathbf{q}_j)}{\sigma_{ij}} \right)^2$$

where $\mathbf{p}$ ($\mathbf{q}$) stands for the alignment (track) parameters,
and m (f) corresponds to the measurement (prediction).

Two algorithms

- MillePede [2]

$\longrightarrow$ fit $\mathbf{p}$ & $\mathbf{q}_j$ simultaneously

- HipPy

$\longrightarrow$ fit them separately & iteratively

Introduction

Track-based alignment

$$\chi^2(\mathbf{p},\mathbf{q}) = \sum_j^{\text{tracks}} \sum_i^{\text{hits}} \left(\frac{m_{ij} - f_{ij}(\mathbf{p},\mathbf{q}_j)}{\sigma_{ij}} \right)^2$$

where $\mathbf{p}$ ($\mathbf{q}$) stands for the alignment (track) parameters,
and m (f) corresponds to the measurement (prediction).

Two algorithms

- MILLEPEDE [2]

$\longrightarrow$ fit $\mathbf{p}$ & $\mathbf{q}_j$ simultaneously

- HIPPY

$\longrightarrow$ fit them separately & iteratively

Challenges

- Extremely large amount of parameters
  $\longrightarrow$ linearise χ^2 and utilise linear algebra and numerical analysis to reduce the problem
- Avoid non-physical distortions due to internal symmetries of the problem
  $\longrightarrow$ a.k.a. Weak Modes (causing invariant, non-physical transformation of the geometry)
- Variations of conditions over time
  $\longrightarrow$ changes of temperature or magnetic field
- **Interplay with local reconstruction**
  $\longrightarrow$ ageing of the detector over time

Weak modes

Definition

A **Weak Mode (WM)** is any transformation such that $\Delta\chi^2 \sim 0$

Weak modes

Definition

A **Weak Mode (WM)** is any transformation such that $\Delta\chi^2 \sim 0$
i.e. it changes **valid** tracks into **other valid** tracks

Weak modes

Definition

A **Weak Mode (WM)** is any transformation such that $\Delta\chi^2 \sim 0$
i.e. it changes **valid** tracks into **other valid** tracks
$\longrightarrow$ **symmetric** detector and collision track topology

Weak modes

Definition

A **Weak Mode (WM)** is any transformation such that $\Delta\chi^2 \sim 0$
i.e. it changes **valid** tracks into **other valid** tracks
$\longrightarrow$ **symmetric** detector and collision track topology

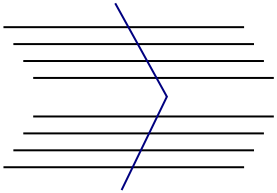

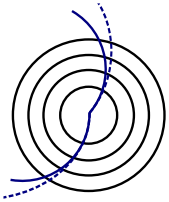

Canonical WMs

	Δr	Δz	r$\Delta\phi$
r	radial	**telescope**	layer rotation
z	bowing	z-expansion	**twist**
ϕ	elliptical	skew	sagitta

Weak modes

Definition

A **Weak Mode (WM)** is any transformation such that $\Delta\chi^2 \sim 0$
i.e. it changes **valid** tracks into **other valid** tracks
$\longrightarrow$ **symmetric** detector and collision track topology

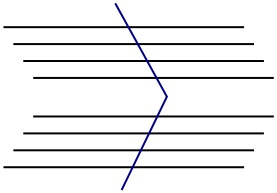

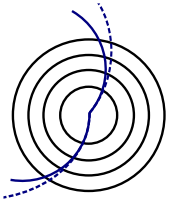

Solution

Use (also) special track topologies:

resonances tracks constrain modules in different directions

cosmic ray muons vertical tracks

(beam halo tracks) (horizontal tracks)

$\longrightarrow$ accumulate them as much as possible!

Canonical WMs

	Δr	Δz	$r\Delta\phi$
r	radial	**telescope**	layer rotation
z	bowing	z-expansion	**twist**
ϕ	elliptical	skew	sagitta

Time variations

Causes

Magnet cycles magnetic field may be switched off for maintenance reasons
$\longrightarrow$ mostly affects the large mechanical structures.

Temperature variations cooling operations after switching on / off the detector
$\longrightarrow$ sensitive effect at module level as well.

Ageing of the modules high-radiation environment
$\longrightarrow$ change of Lorentz drift inside of the silicon modules (although mostly – but not entirely – covered by the pixel calibration).

Time variations

Causes

Magnet cycles magnetic field may be switched off for maintenance reasons
$\longrightarrow$ mostly affects the large mechanical structures.

Temperature variations cooling operations after switching on / off the detector
$\longrightarrow$ sensitive effect at module level as well.

Ageing of the modules high-radiation environment
$\longrightarrow$ change of Lorentz drift inside of the silicon modules (although mostly – but not entirely – covered by the pixel calibration).

Solution 1 (applied during data taking)

Re-align as often as possible, with limited statistics of special track topologies.

Time variations

Causes

Magnet cycles magnetic field may be switched off for maintenance reasons
$\longrightarrow$ mostly affects the large mechanical structures.

Temperature variations cooling operations after switching on / off the detector
$\longrightarrow$ sensitive effect at module level as well.

Ageing of the modules high-radiation environment
$\longrightarrow$ change of Lorentz drift inside of the silicon modules (although mostly – but not entirely – covered by the pixel calibration).

Solution 1 (applied during data taking)

Re-align as often as possible, with limited statistics of special track topologies.

Solution 2 (applied for end-of-year or Legacy reprocessing)

Introduce hierarchy & align separately:

- **absolute** positions of **High-Level Structure (HLS)** with time-dependence;
- **relative** positions of **modules** to the HLSs without time-dependence.

$\longrightarrow$ Include time dependence while avoiding splitting samples of special tracks.
NB: definition of HLSs depends on the case (*e.g.* typically subdetectors, but not always).

During Run-2

Start-up

Along the year

Start-up

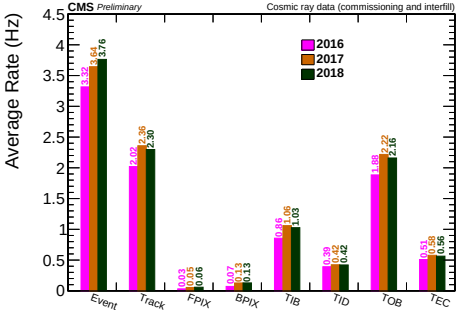

With first cosmic tracks

- **HLS alignment** before first pp collisions (at least in pixel detector).
- Each year, **roughly half of the cosmics** with magnetic field are taken during commissioning.
- If **combining with cosmics at $0\ \mathrm{T}$**, alignment at Module Level (actually sensor level) (ML) in pixel is also possible.

Start-up

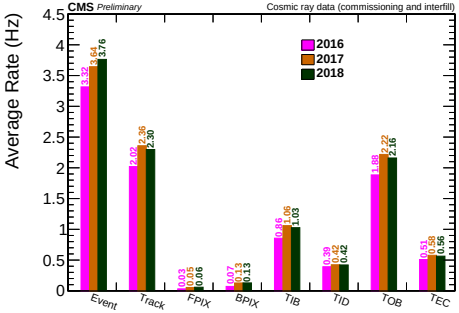

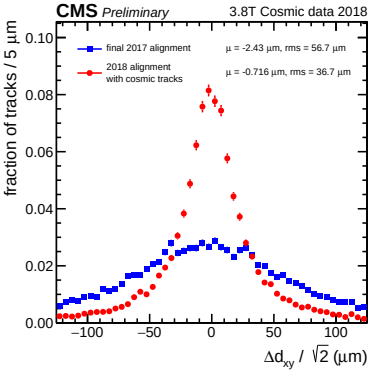

With first cosmic tracks

- **HLS alignment** before first pp collisions (at least in pixel detector).
- Each year, **roughly half of the cosmics** with magnetic field are taken during commissioning.
- If **combining with cosmics at 0 T**, alignment at Module Level (actually sensor level) (ML) in pixel is also possible.

Cosmic ray muons (MTS)

- Consider **muon tracks traversing** the pixel detector.
- **Split** the track into two subtracks close to the origin.
- **Compare** (sub)track variables.

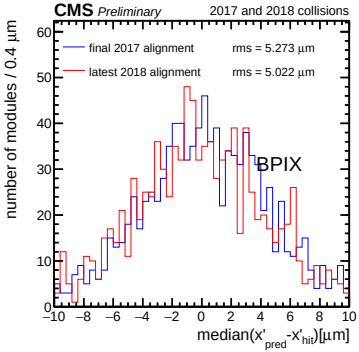

Start-up

With first collision tracks

- Quick reaction to avoid time-dependent alignment with **more delicate configuration**.
- Alignment precision improves with **larger statistics**.
- However **no $Z \to \mu\mu$ data**, so full-ML alignment is still difficult to achieve.

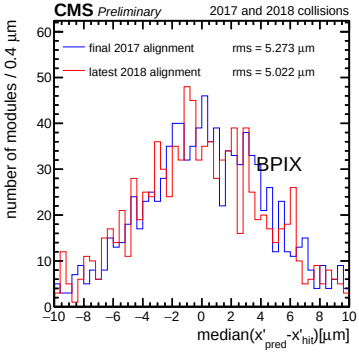

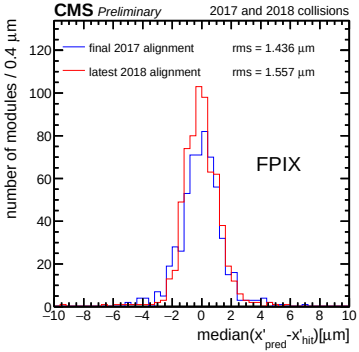

Start-up

With first collision tracks

- Quick reaction to avoid time-dependent alignment with **more delicate configuration**.
- Alignment precision improves with **larger statistics**.
- However **no $Z \to \mu\mu$ data**, so full-ML alignment is still difficult to achieve.

Tracking performance (DMR)

- Measuring the **residual of the hits belonging to a track** (each time refitted without the hit under scrutiny).
- Expect distribution peaked around 0.

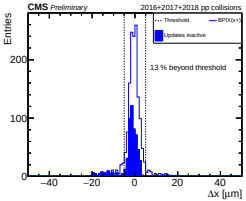

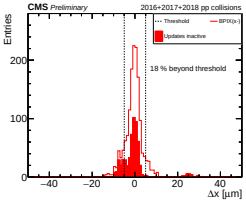

Along the year

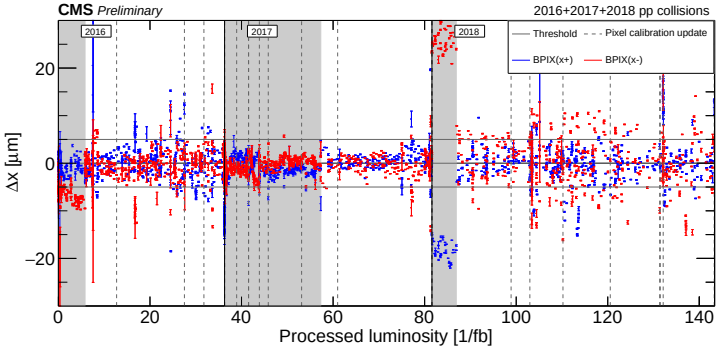

Automated alignment [3]

Only activated once we are confident in the alignment (white background in figure):

- **Align as soon as possible** with most recent data (without special track topology).
- Only for positions of BPIX **half-barrels** & FPIX **half-cylinders**.
- Can be derived and applied in < 48 h.
- However **cannot correct for radiation effects**.

⟶ A few **human interventions** per year are still necessary.

Legacy

Overview
Tracking & vertexing
Interplay with local reco
Further results

Overview

Legacy Reprocessing

Around one year of intense work to produce ultimate Run 2 alignment (2016-2018), corresponding to $\sim 140\ \mathrm{fb}^{-1}$:

- For **each year**, the whole data is aligned in a **single, global fit** in order to accumulate enough cosmic rays ($2 - 4M$ in practice), since this is the limiting factor.
- Coping with residual systematic changes in hit positions due to **radiation** with appropriate hierarchy of alignment parameters.
- **Largest alignment fits** to date in terms of number of parameters to align, with up to $\sim 700k$ parameters!

$\longrightarrow$ ~ 220 **geometries** over the three years to cover significant changes over time.

Overview

Legacy Reprocessing

Around one year of intense work to produce ultimate Run 2 alignment (2016-2018), corresponding to $\sim 140\ \mathrm{fb}^{-1}$:

- For **each year**, the whole data is aligned in a **single, global fit** in order to accumulate enough cosmic rays ($2-4M$ in practice), since this is the limiting factor.
- Coping with residual systematic changes in hit positions due to **radiation** with appropriate hierarchy of alignment parameters.
- **Largest alignment fits** to date in terms of number of parameters to align, with up to $\sim 700k$ parameters!

$\longrightarrow$ ~ 220 **geometries** over the three years to cover significant changes over time.

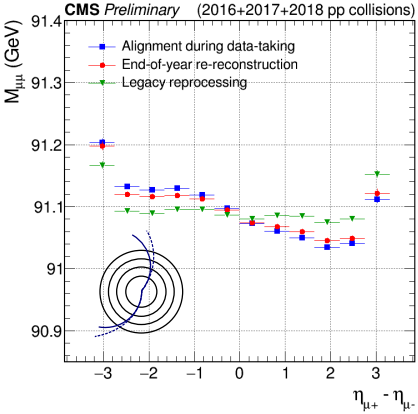

Figure

Direct, significant impact on the uniformity of track p_T response, hence on M_Z measurement.

NB: figure does not include further momentum scale corrections beyond changes of alignment.

https://twiki.cern.ch/twiki/bin/view/CMSPublic/CMSTrackerPerformanceResultsForFullRun2LegacyReprocessing

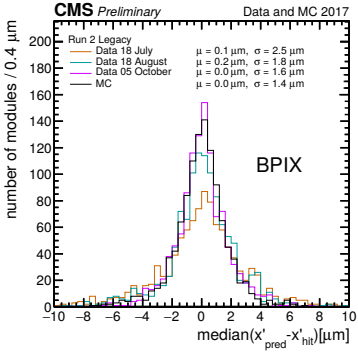

Tracking & vertexing

Tracking performance (DMR)

- Repeating track performance as done at start-up.
- Can be performed **separately for inward- and outward-pointing modules** (see next slides & back-up).

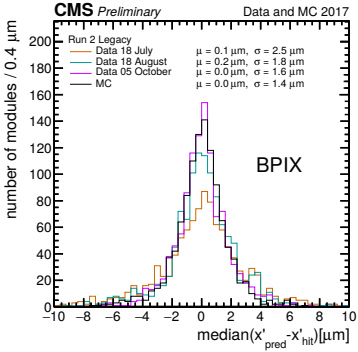

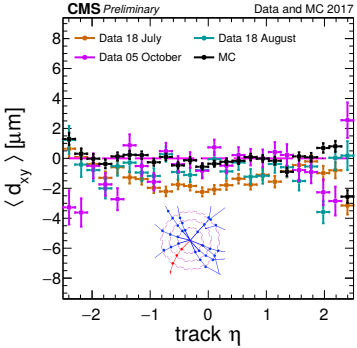

Tracking & vertexing

Tracking performance (DMR)

- Repeating track performance as done at start-up.
- Can be performed **separately for inward- and outward-pointing modules** (see next slides & back-up).

Vertexing performance (PV)

- Measuring **IP of tracks belonging to a vertex** (each time refitted without the track under scrutiny).
- Expect flat distribution centered at 0.

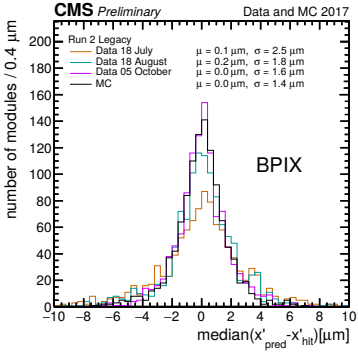

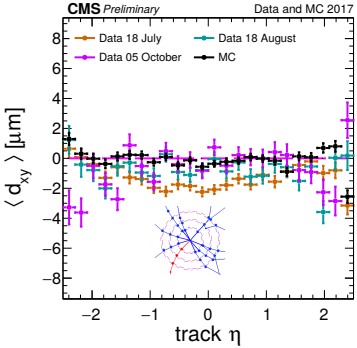

Tracking & vertexing

Tracking performance (DMR)

- Repeating track performance as done at start-up.
- Can be performed **separately for inward- and outward-pointing modules** (see next slides & back-up).

Vertexing performance (PV)

- Measuring **IP of tracks belonging to a vertex** (each time refitted without the track under scrutiny).
- Expect flat distribution centered at 0.

Simulation

- During data taking, we usually derive them before obtaining the final alignment.
- For the Legacy alignment, we derived the misalignment scenarios **after** obtaining the alignment in the data.

Interplay with local reco

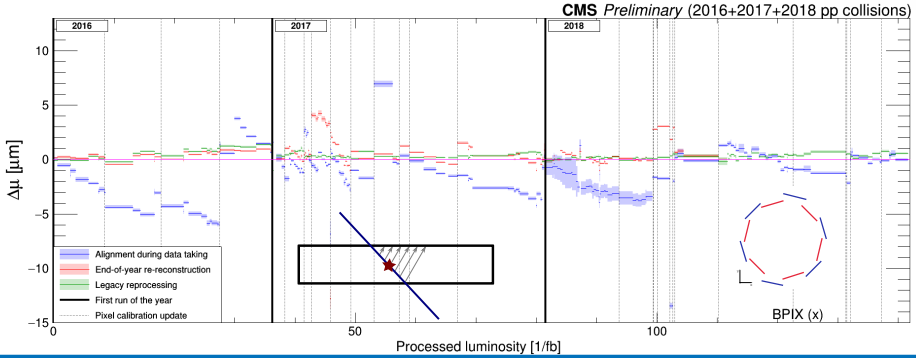

Ageing of the modules

- **Local reco** is affected by the accumulated radiation.

Interplay with local reco

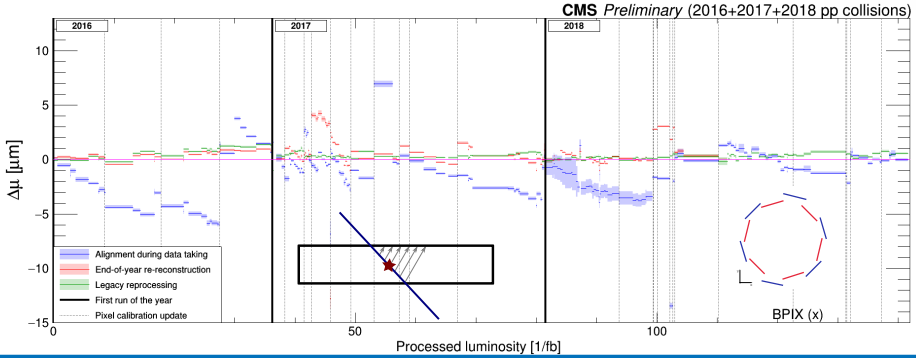

Ageing of the modules

- **Local reco** is affected by the accumulated radiation.
- Alignment is sensitive to changes in the **Lorentz drift** induced by radiation accumulated in $\sim 1\ \mathrm{fb}^{-1}$, while the pixel local reconstruction calibration can only be performed after $\sim 10\ \mathrm{fb}^{-1}$, hence the need to absorb residual effect.

Interplay with local reco

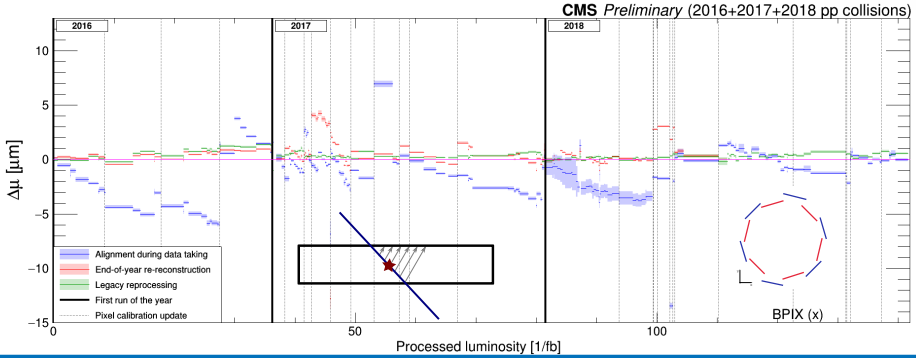

Ageing of the modules

- **Local reco** is affected by the accumulated radiation.
- Alignment is sensitive to changes in the **Lorentz drift** induced by radiation accumulated in $\sim 1\ \mathrm{fb}^{-1}$, while the pixel local reconstruction calibration can only be performed after $\sim 10\ \mathrm{fb}^{-1}$, hence the need to absorb residual effect.
- BPIX modules are arranged in ladders successively facing inward and outward, hence the **systematic shift occurs in opposite directions**.

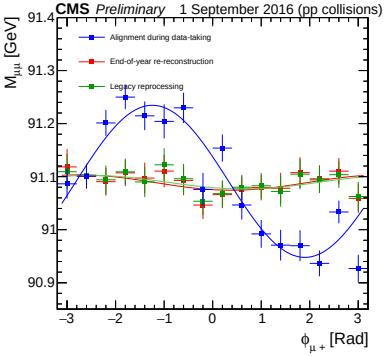

Further results

Selected figure: $M_Z(\phi_\mu)$

- At first order, we fit deviations with a sine curve for each of the ~ 220 periods and for each of the geometries.
- We show the amplitude of the sine as a function of the processed luminosity.
- Direct impact on reconstruction of muon tracks, especially at high p_T.

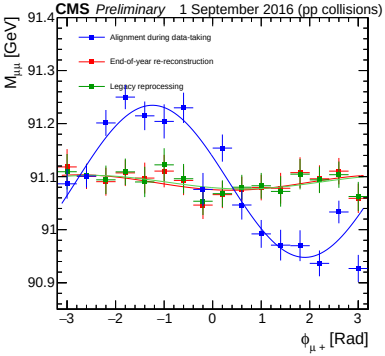

Further results

Selected figure: $M_Z(\phi_\mu)$

- At first order, we fit deviations with a sine curve for each of the ~ 220 periods and for each of the geometries.
- We show the amplitude of the sine as a function of the processed luminosity.
- Direct impact on reconstruction of muon tracks, especially at high p_T.

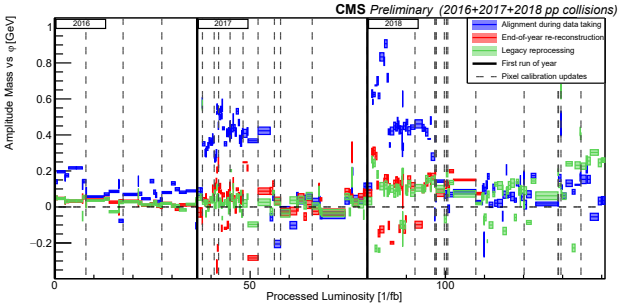

Other results
(see back-up)

- Movements of modules
- Overlap of modules
- Impact parameter trends
- Alignment errors
- BPIX barycentre
- ...

Run 3

Start-up

Prospects

Run 3

Start-up

Long Shutdown 2

- Detector was opened for maintenance.
- BPIX L1 was fully replaced.

Run 3
Start-up

Long Shutdown 2

- Detector was opened for maintenance.
- BPIX L1 was fully replaced.

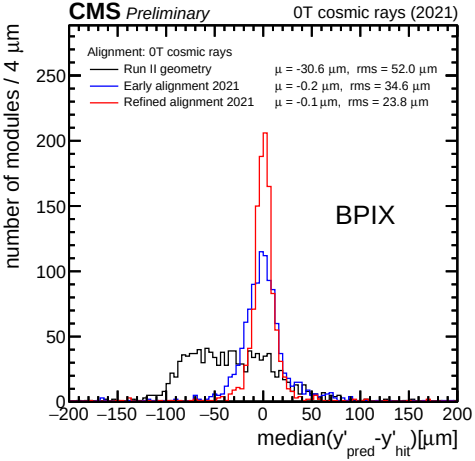

CRUZET

early alignment 120k tracks, align half-barrels in BPIX and half-cylinders in FPIX.

refined alignment 1.5M tracks, align ladders in BPIX and half-cylinders in FPIX.

Run 3

Start-up

Long Shutdown 2

- Detector was opened for maintenance.
- BPIX L1 was fully replaced.

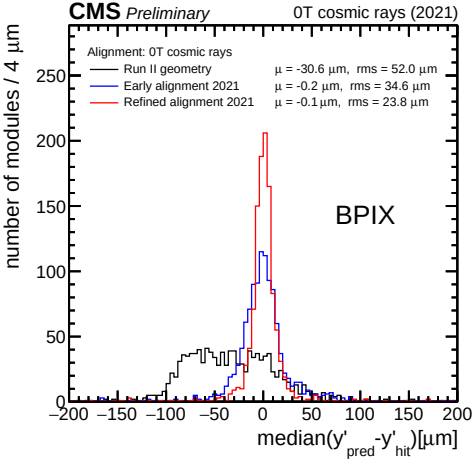

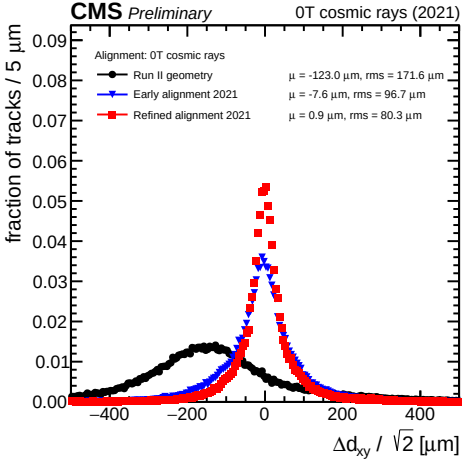

CRUZET

early alignment 120k tracks, align half-barrels in BPIX and half-cylinders in FPIX.

refined alignment 1.5M tracks, align ladders in BPIX and half-cylinders in FPIX.

Run 3

Prospects

Coming months

CRAFT21	A few days in Autumn
CRAFT22	A few weeks in Winter
pp commissioning	*id.*
physics runs	Spring onwards

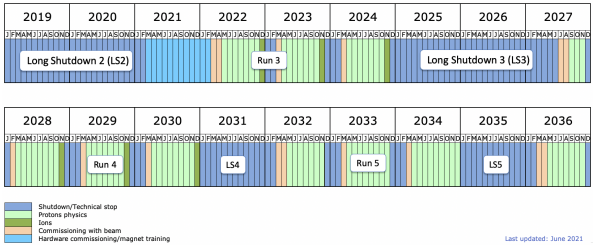

Run 3

Prospects

Coming months

CRAFT21	A few days in Autumn
CRAFT22	A few weeks in Winter
pp commissioning	*id.*
physics runs	Spring onwards

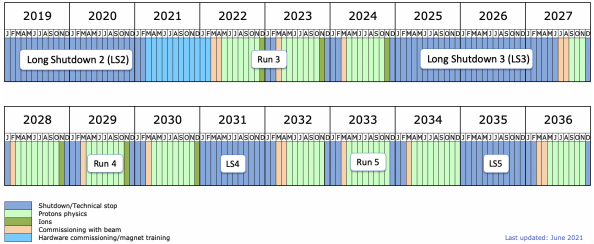

Online alignment

- Expecting **similar data taking conditions** as during Run 2.
- Planning to run **automated alignment of ladders and panels** (instead of HLS as in Run 2) to reduce need and frequency of human interventions.
- **Emulation with Run 2 data** stored on disk shows promise.

Summary & Conclusions

Summary & Conclusions

- **General concepts** of tracker alignment were explained, namely track-based alignment, time variations, intrinsic symmetries, and **interplay with local reconstruction**.
- **Strategies** during and after data taking were addressed.
- Improvements of the alignment with the **Legacy reprocessing** were shown, including flattening of Z boson mass distributions, track-hit residuals, impact parameter, etc.
- First results & prospects for **Run 3** were discussed.

NB: extensive amount of results (see back-up)

$\rightarrow$ **paper in preparation!**

Summary & Conclusions

- **General concepts** of tracker alignment were explained, namely track-based alignment, time variations, intrinsic symmetries, and **interplay with local reconstruction**.
- **Strategies** during and after data taking were addressed.
- Improvements of the alignment with the **Legacy reprocessing** were shown, including flattening of Z boson mass distributions, track-hit residuals, impact parameter, etc.
- First results & prospects for **Run 3** were discussed.

NB: extensive amount of results (see back-up)

$\rightarrow$ **paper in preparation!**

Thank you for your attention!

Back-up

Abstract

In order to provide optimal reconstruction of charged tracks, the positions of the nearly twenty-thousands silicon sensors of the central tracking system of the CMS detector must be determined at a better precision than their intrinsic resolution, under a procedure called alignment. At CMS, the alignment also includes the orientation and surface deformations of the sensors. Data-driven methods to carefully align the detector and validate the alignment are presented in the context of the legacy alignment for CMS Run 2 data, corresponding to the data accumulated from 2016 to 2018. Systematic distortions are discussed, such as weak modes and variations of the conditions during data taking over time, in particular effects related to the radiation damages.

Tracker

Pixel Tracker

Layer	#TBM/module	#cores/TBM	#channels/core	#ROCs/channel
1	2	2	2	2
2	1	2	2	4
3/4	1	2	1	8

Tracker

Strip Tracker

Layer	Radius /mm	Type	#Modules	Pitch /μ	Strips
TIB 1	250	double-sided	336	80	768
TIB 2	340	double-sided	456	80	7768
TIB 3	430	single-sided	552	120	7512
TIB 4	520	single-sided	648	120	7512
TOB 5	610	double-sided	504	122/183	768/512
TOB 6	696	double-sided	576	122/183	768/512
TOB 7	782	single-sided	648	183	512
TOB 8	868	single-sided	720	183	512
TOB 9	965	single-sided	792	122	768
TOB 10	1080	single-sided	888	122	768

Tracker

Strip Tracker

Layer	Radius /mm	Type	#Modules	Pitch /μ	Strips
TID 1	277	double-sided	144	$81 \ldots 112$	768
TID 2	367	double-sided	144	$113 \ldots 143$	768
TID 3	447	single-sided	240	$124 \ldots 158$	512
TEC 1	277	double-sided	144	$81 \ldots 112$	768
TEC 2	367	double-sided	288	$113 \ldots 143$	768
TEC 3	447	single-sided	640	$124 \ldots 158$	512
TEC 4	562	single-sided	1008	$113 \ldots 139$	512
TEC 5	677	double-sided	720	$126 \ldots 156$	768
TEC 6	891	single-sided	1008	$163 \ldots 205$	512
TEC 7	991	single-sided	1440	$140 \ldots 172$	512

MillePede-2 I

Reformulation

We re-write & linearise the aforementioned χ^2:

$$\chi^2(\mathbf{A}) = \sum_k \left(\frac{m_k - \mathbf{d}_k^\mathsf{T} \cdot \mathbf{A}}{\sigma_k} \right)^2 \tag{1}$$

At the minimum:

$$\underbrace{\left(\sum_k \frac{(\mathbf{d}_k \cdot \mathbf{d}_k^\mathsf{T})}{\sigma_k^2} \right)}_{\equiv \mathbf{C}} \times \mathbf{A} = \underbrace{\sum_k \frac{m_k}{\sigma_k^2} \mathbf{d}_k}_{\equiv \mathbf{B}} \tag{2}$$

$\longrightarrow$ matrix inversion problem with a huge matrix $\mathbf{C}$...

Number of parameters

$\sim 200k$ alignment parameters $+ \mathcal{O}(10M)$ track parameters

MillePede-2 II

A bit of block matrix algebra

- Distinguish among **local** (track) and **global** (sensor) parameters:

$$\mathbf{a}^\intercal \cdot \mathbf{d} = \underbrace{\sum_{i=0}^{n} a_j \cdot d_j}_{\text{global parameters}} + \underbrace{\sum_{i=0}^{N\cdot\nu} \alpha_j \cdot \delta_j}_{\text{local parameters}}$$

  for N measurements and ν parameters per track.

- Partition the **sparse** matrix $\mathbf{C}$ into blocks for **local** and **global** parameters:

$$\left(\begin{array}{c|ccc} \sum \mathbf{G}_i & \cdots & \Gamma_i & \cdots \\ \hline \vdots & \ddots & 0 & 0 \\ \Gamma_i^\intercal & 0 & \mathbf{L}_i & 0 \\ \vdots & 0 & 0 & \ddots \end{array}\right) \left(\begin{array}{c} \mathbf{a} \\ \hline \vdots \\ \alpha_i \\ \vdots \end{array}\right) = \left(\begin{array}{c} \sum \mathbf{b}_i \\ \hline \vdots \\ \beta_i \\ \vdots \end{array}\right)$$

MillePede-2 III

A bit of block matrix algebra (continued)

- (Re)define:

  local solutions $\alpha_i^* \equiv \mathbf{L}_i^{-1}\mathbf{b}_i$
  source term $\mathbf{b}' \equiv \sum (\mathbf{b}_i - \mathbf{L}_i\alpha_i^*)$
  inverse of Schur complement $\mathbf{C}' \equiv \sum \left(\mathbf{G}_i - \Gamma_i\mathbf{L}_i^{-1}\Gamma_i^\intercal\right)$

Then the problem simplifies to a "smaller" matrix inversion problem:

$$\mathbf{C}'\mathbf{a} = \mathbf{b}' \tag{3}$$

$\longrightarrow$ many steps are parallelised using `OpenMP`.

Number of parameters

- Given N measurements, we reduce the computing time of the matrix inversion from $\propto (n + N\nu)^3$ to "only" $\propto n^3$!
- Of course, the reduction of the matrix size is not instantaneous, but one can know envisage very large samples to perform the alignment with limited / controlled impact on the computation time.

MillePede-2 IV

MINRES-QLP [4]

- Further trick when $n \gg \mathcal{O}(1k - 10k)$.
- Minimise iteratively $||\mathbf{C}'\mathbf{a} - \mathbf{b}'||$.
- Number of iteration rarely exceeds 2000.

$\longrightarrow$ reduces the necessary computing power to $\mathcal{O}(n^2 \times n_{\text{it}})$
(Here, a solution using GPUs is being investigated.)

Cases

large-mechanical structures $n \approx \mathcal{O}(10 - 100)$, $\mathcal{O}(< 1\ \text{h})$ & $\mathcal{O}(1\ \text{GB})$

pixel sensor-level $n \approx \mathcal{O}(1k - 10k)$, $\mathcal{O}(1\ \text{h})$ & $\mathcal{O}(10\ \text{GB})$

pixel + strip sensor-level $n \approx \mathcal{O}(100k)$, $\mathcal{O}(10\ \text{h})$ & $\mathcal{O}(100\ \text{GB})$

$\longrightarrow$ pure inversion can be used in the two first cases, but usually not in the third...

Results

Terminology

selection IOV one of the ~ 220 geometries

average lumi-average performance over the ~ 220 geometries

trend performance as a function of the processed luminosity

Overview of public results

	selected IOV	average	trends
Geometry comparison	x		x
DMRs & DRNRs	x	x	x
PV	x		x
overlap	x		x
$Z \to \mu\mu$	x	x	x
MTS	x	x	
APEs	x		x
barycentre			x

https://twiki.cern.ch/twiki/bin/view/CMSPublic/CMSTrackerPerformanceResultsForFullRun2LegacyReprocessing

Cosmic rates

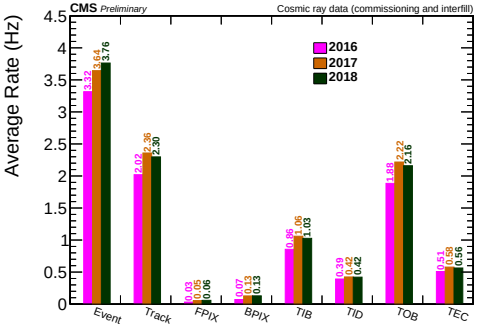

Average rates of cosmic ray data (in Hz) recorded by the CMS tracker during the years 2016, 2017, and 2018, calculated including all commissioning and interfill runs. Events are required to have at least one track with a minimum of 7 hits, and at least two hits measured in either pixel detector or stereo strip modules (2D measurement). For the event rate (first bin), tracks are reconstructed by at least one out of three reconstruction algorithms (CMS Collaboration, Alignment of the CMS Silicon Tracker during Commissioning with Cosmic Rays.(2010) J. Inst. 5 T03009). For the track rate calculation instead (all other bins), tracks reconstructed by one of the three reconstruction algorithms are considered as the input for the tracker alignment procedure. Track rates per partition are obtained by requiring tracks to have at least one valid hit in each partition. The statistical uncertainty on the measured rates is negligible and hence not shown in the plot.

Geometry comparison

Selected IOV

Difference in the positions of the modules between the alignment constants used during data taking and the alignment constants obtained after aligning the tracker. The change in the z coordinate between the constants obtained after aligning the tracker and the alignment constants used during data taking is shown as a function of the coordinate r in the alignment constants used during data taking. Each point represents a module. The colours correspond to the different sub-detectors of the tracker, and match the colours used in the tracker layout shown above. The alignment constants are time-dependent, those used here were obtained for data taken from 18 to 19 May 2018. The large spread in movements in the tracker end-caps is a feature of the algorithm used for the alignment. The algorithm cannot constrain the positions of modules far away from the interaction point along the longitudinal axis as tightly as for modules which are closer to the interaction point along the longitudinal axis. This module position comparison shows that the alignment procedure shifts the position of the BPIX detector.

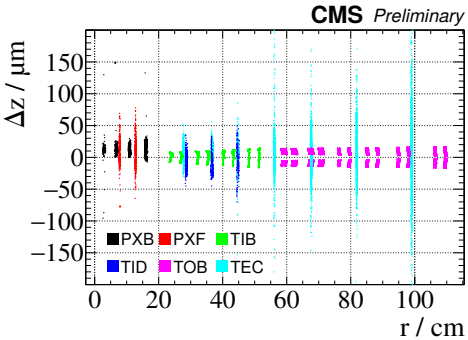

Geometry comparison

Trends

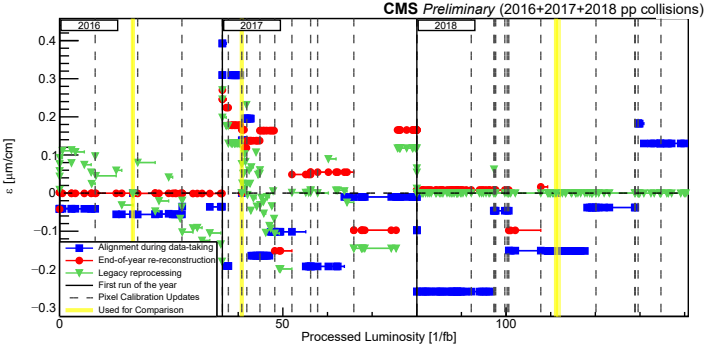

The slope (ϵ) given by fitting the difference in the measured z position (Δz) vs z for each module in the Barrel Pixel with respect to a reference alignment constraint, to a linear function of the form $\epsilon z + b$ as a function of processed luminosity. A non-zero ϵ indicates a z-expansion of the geometry relative to the reference geometry. $\epsilon = \pm\ 0.1$ corresponds to a z-expansion/contraction of $\mp\ 2.6\ \ \mathrm{mm}$ at z = 26cm. The vertical black solid lines indicate the first processed run for 2016, 2017, and 2018 data-taking period, respectively. The vertical dotted lines indicate a change in the pixel tracker calibration. The blue points correspond to the results with the alignment constants used during data-taking, the red points show the results with the alignment constants used during the 2016, 2017, and 2018 EOY re-reconstruction (notice there is no EOY re-reconstruction for the last $33\ \mathrm{fb}^{-1}$ of data-taking), the green points show the results with the alignment constants as obtained in the Run 2 Legacy alignment procedure. During the LHC shutdown in winter 2016/17, the pixel detector was replaced [3]. In 2016, 2017, and 2018 we compare to the Legacy Reprocessing geometry for pp collisions on 8 August 2016, 10 July 2017, and 8 August 2018 respectively.

Geometry comparison

Trends

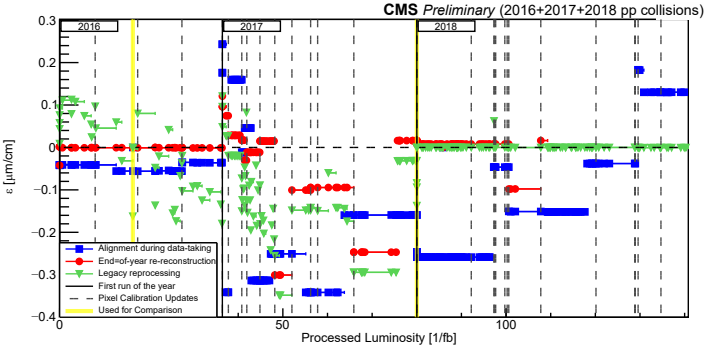

The slope (ϵ) given by fitting the difference in the measured z position (Δz) vs z for each module in the Barrel Pixel with respect to a reference alignment constraint, to a linear function of the form $\epsilon z + b$ as a function of processed luminosity. The shift between 2017 and 2018 can be caused by some global shift of the large scale structure of the Barrel Pixel along the z-axis. $\epsilon = \pm\ 0.1$ corresponds to a z-expansion/contraction of $\mp\ 2.6\ \ \mathrm{mum}$ at z = 26cm relative to the reference alignment. The vertical black solid lines indicate the first processed run for 2016, 2017, and 2018 data-taking period, respectively. The vertical dotted lines indicate a change in the pixel tracker calibration. The blue points correspond to the results with the alignment constants used during data-taking, the red points show the results with the alignment constants used during the 2016, 2017, and 2018 EOY re-reconstruction (notice there is no EOY re-reconstruction for the last $33\ \mathrm{fb}^{-1}$ of data-taking), the green points show the results with the alignment constants as obtained in the Run 2 Legacy alignment procedure. During the LHC shutdown in winter 2016/17, the pixel detector was replaced [3]. In 2016,2017, and 2018 we compare to the Legacy Reprocessing geometry for pp collisions on 8 August 2016, 10 July 2017, and August 8 2018 respectively.

Geometry comparison

Trends

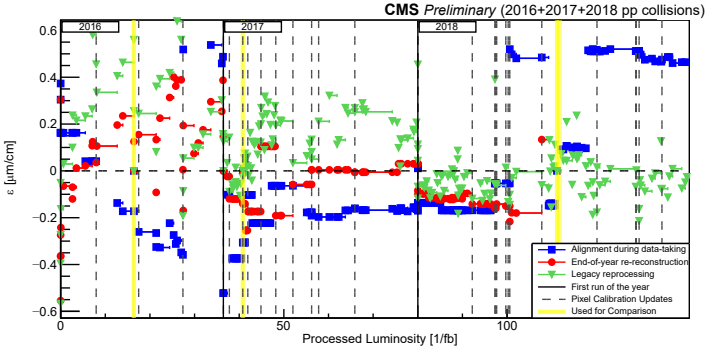

The slope (ϵ) given by fitting the difference in the measured r position (Δr))vs r for each module in the Barrel Pixel with respect to a reference alignment constraint, to a linear function of the form $\epsilon r + b$ as a function of processed luminosity. A non-zero ϵ indicates a radial expansion of the geometry relative to the reference geometry. $\epsilon = \pm$ 0.2 corresponds to a radial expansion/contraction of $\mp$ 3.2 mum at r = 16 cm. The vertical black solid lines indicate the first processed run for 2016, 2017, and 2018 data-taking period, respectively. The vertical dotted lines indicate a change in the pixel tracker calibration. The blue bands correspond to the results with the alignment constants used during data-taking, the red bands show the results with the alignment constants used during the 2016, 2017, and 2018 EOY re-reconstruction (notice there is no EOY re-reconstruction for the last $33\ \mathrm{fb}^{-1}$ of data-taking), the green bands show the results with the alignment constants as obtained in the Run 2 Legacy alignment procedure. During the LHC shutdown in winter 2016/17, the inner component (pixel detector) of the CMS tracking detector was replaced [3]. In 2016,2017, and 2018 we compare to the Legacy Reprocessing geometry for pp collisions on 8 August 2016, 10 July 2017, and August 8 2018 respectively.

Geometry comparison

Trends

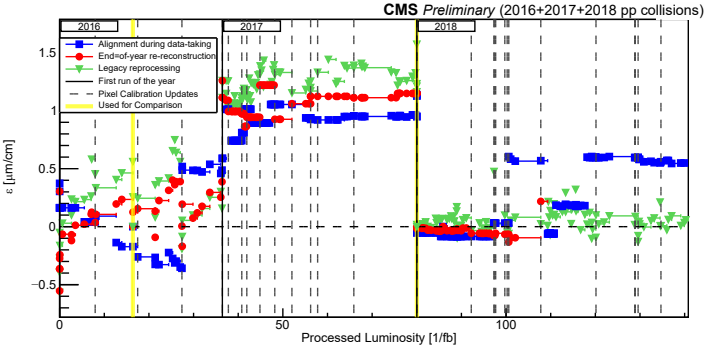

The slope (ϵ) given by fitting the difference in the measured r position (Δr) vs r for each module in the Barrel Pixel with respect to a reference alignment constraint, to a linear function of the form $\epsilon R + b$ as a function of processed luminosity. The vertical black solid lines indicate the first processed run for 2016, 2017, and 2018 data-taking period, respectively. The shift between 2017 and 2018 can be caused by some global shift of the two shells of the Barrel Pixel such as expansion or contraction along the x-axis.$\epsilon = \pm$ 0.2 corresponds to a radial expansion/contraction of $\mp$ 3.2 mum at r = 16 cm. The vertical dotted lines indicate a change in the pixel tracker calibration. The blue bands correspond to the results with the alignment constants used during data-taking, the red bands show the results with the alignment constants used during the 2016, 2017, and 2018 EOY re-reconstruction (notice there is no EOY re-reconstruction for the last $33\ \mathrm{fb}^{-1}$ of data-taking), the green bands show the results with the alignment constants as obtained in the Run 2 Legacy alignment procedure. During the LHC shutdown in winter 2016/17, the inner component (pixel detector) of the CMS tracking detector was replaced [3]. In 2016 we compare to the Legacy Reprocessing geometry for pp collisions on 8 August 2016 and in 2017 and 2018 we compare to the Legacy Reprocessing geometry for pp collisions on 05 April 2018.

Geometry comparison

Trends

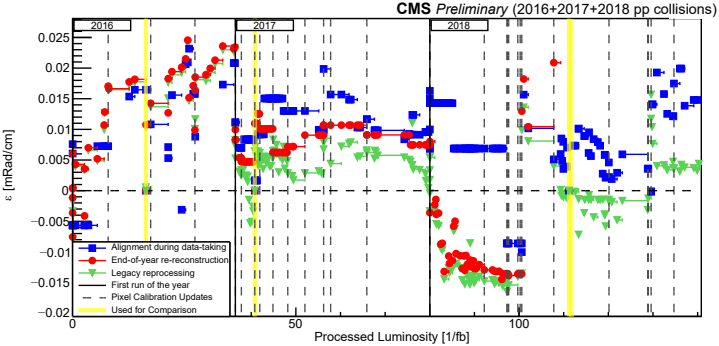

The slope (ϵ) given by fitting the difference in the measured r position ($\Delta\phi$) vs z for each module in the Barrel Pixel with respect to a reference alignment constraint, to a linear function of the form $\epsilon Z + b$ as a function of processed luminosity. A non-zero ϵ indicates a twist of the geometry relative to the reference geometry. $\epsilon = \pm$ 0.01 corresponds to a twist of $\mp$ 2.6 $mrad$ (Constant at all r). The vertical black solid lines indicate the first processed run for 2016, 2017, and 2018 data-taking period, respectively. The vertical dotted lines indicate a change in the pixel tracker calibration. The blue points correspond to the results with the alignment constants used during data-taking, the red bands show the results with the alignment constants used during the 2016, 2017, and 2018 EOY re-reconstruction (notice there is no EOY re-reconstruction for the last $33\ \mathrm{fb}^{-1}$ of data-taking), the green points show the results with the alignment constants as obtained in the Run 2 Legacy alignment procedure. During the LHC shutdown in winter 2016/17, the pixel detector was replaced [3]. In 2016, 2017, and 2018 we compare to the Legacy Reprocessing geometry for pp collisions on 8 August 2016, 10 July 2017, and 8 August 2018 respectively.

Geometry comparison

Trends

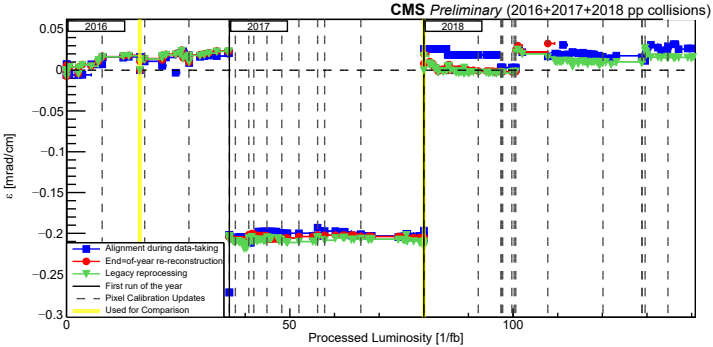

The slope (ϵ) given by fitting the difference in the measured r position (Δr) vs z for each module in the Barrel Pixel with respect to a reference alignment constraint, to a linear function of the form $\epsilon z + b$ as a function of processed luminosity. The shift between 2017 and 2018 can be caused by some global shift of the shells of the Barrel Pixel such as a non zero angle of a shell with respect to the z-axis in the y-z plane. $\epsilon = \pm 0.01$ corresponds to a twist of $5 \pm 2.6\ \mathrm{mrad}$ (constant at all r). The vertical black solid lines indicate the first processed run for 2016, 2017, and 2018 data-taking period, respectively. The vertical dotted lines indicate a change in the pixel tracker calibration. The blue points correspond to the results with the alignment constants used during data-taking, the red points show the results with the alignment constants used during the 2016, 2017, and 2018 EOY re-reconstruction (notice there is no EOY re-reconstruction for the last $33\ \mathrm{fb}^{-1}$ of data-taking), the green points show the results with the alignment constants as obtained in the Run 2 Legacy alignment procedure. During the LHC shutdown in winter 2016/17, the pixel detector was replaced [3]. In 2016 we compare to the Legacy Reprocessing geometry for pp collisions on 8 August 2016 and in 2017 and 2018 we compare to the Legacy Reprocessing geometry for pp collisions on 05 April 2018.

Tracking

Distributions of medians of unbiased track-hit residuals. Each track is refitted using the alignment constants under consideration, and the hit prediction for each module is obtained from all of the other track hits. The median of the distribution of unbiased hit residuals is then taken for each module and is histogrammed. The width of this distribution of the medians of residuals (DMR) is a measure of the local precision of the alignment results; deviations from zero indicate biases.

Tracking

Selected IOV

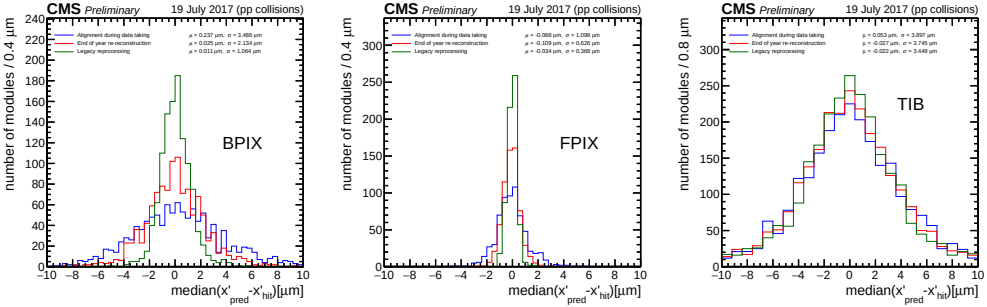

The distribution of median residuals is plotted for the local-x (x') direction individually for each part of the tracker. As an example, run from July 2017 was selected. The blue points correspond to the results with the alignment constants used during data-taking, the red points show the results with the alignment constants used during 2017 EOY re-reconstruction, the green points show the results with the alignment constants as obtained in the Run 2 Legacy alignment procedure. The position of the pixel detector is known to be very sensitive to the change of conditions, *e.g.* temperature and magnetic field. The quoted means μ and standard deviations σ are the parameters of a Gaussian fit to the distributions. They show an improvement for the Legacy reprocessing over the alignment used in data taking or EOY re-reconstruction.

Tracking

Selected IOV

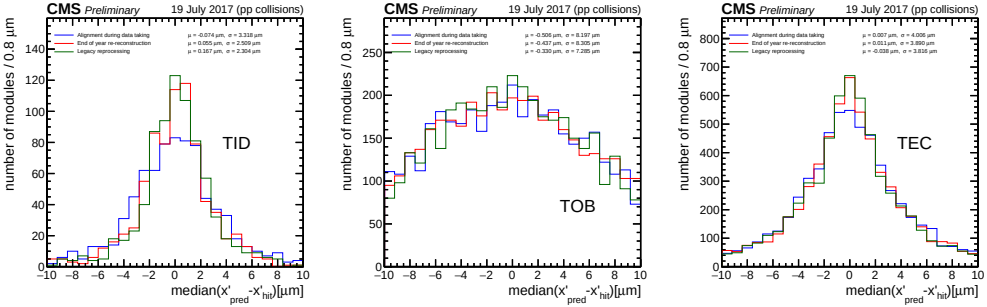

The distribution of median residuals is plotted for the local-x (x') direction individually for each part of the tracker. As an example, run from July 2017 was selected. The blue points correspond to the results with the alignment constants used during data-taking, the red points show the results with the alignment constants used during 2017 EOY re-reconstruction, the green points show the results with the alignment constants as obtained in the Run 2 Legacy alignment procedure. The position of the pixel detector is known to be very sensitive to the change of conditions, *e.g.* temperature and magnetic field. The quoted means μ and standard deviations σ are the parameters of a Gaussian fit to the distributions. They show an improvement for the Legacy reprocessing over the alignment used in data taking or EOY re-reconstruction.

Tracking

Selected IOV

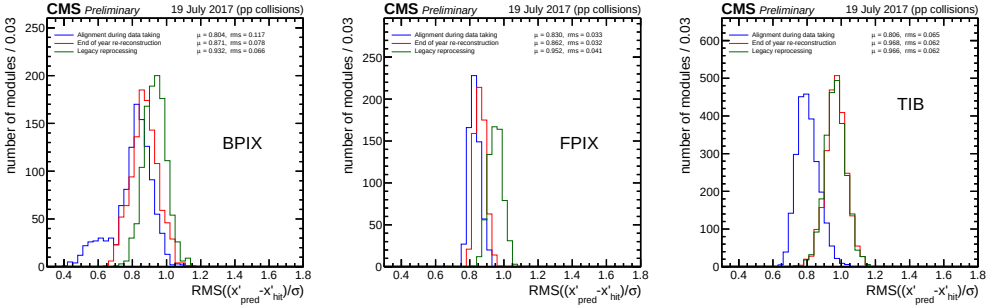

The distribution of RMS normalized residuals is plotted for the local-x (x') direction individually for each part of the tracker. As an example, run from July 2017 was selected. The blue points correspond to the results with the alignment constants used during data-taking, the red points show the results with the alignment constants used during 2017 EOY re-reconstruction, the green points show the results with the alignment constants as obtained in the Run 2 Legacy alignment procedure. The position of the pixel detector is known to be very sensitive to the change of conditions, *e.g.* temperature and magnetic field. The quoted means μ and standard deviations σ are the parameters of a Gaussian fit to the distributions. They show an improvement for the Legacy reprocessing over the alignment used in data taking or EOY re-reconstruction.

Tracking

Selected IOV

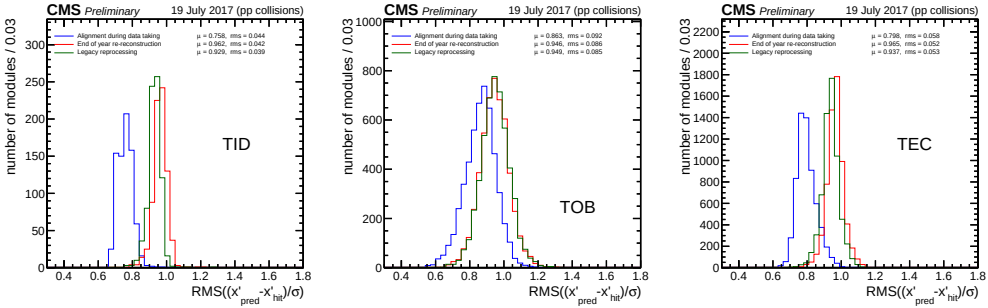

The distribution of RMS normalized residuals is plotted for the local-x (x') direction individually for each part of the tracker. As an example, run from July 2017 was selected. The blue points correspond to the results with the alignment constants used during data-taking, the red points show the results with the alignment constants used during 2017 EOY re-reconstruction, the green points show the results with the alignment constants as obtained in the Run 2 Legacy alignment procedure. The position of the pixel detector is known to be very sensitive to the change of conditions, *e.g.* temperature and magnetic field. The quoted means μ and standard deviations σ are the parameters of a Gaussian fit to the distributions. They show an improvement for the Legacy reprocessing over the alignment used in data taking or EOY re-reconstruction.

Tracking

Selected IOV

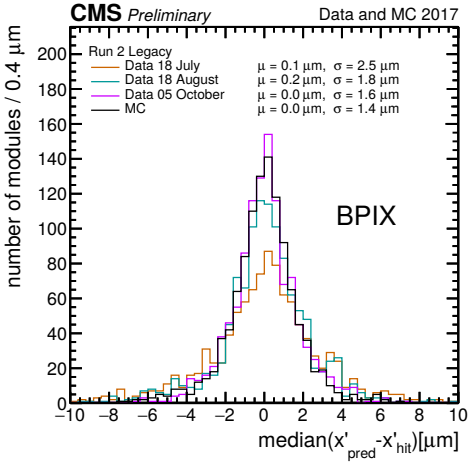

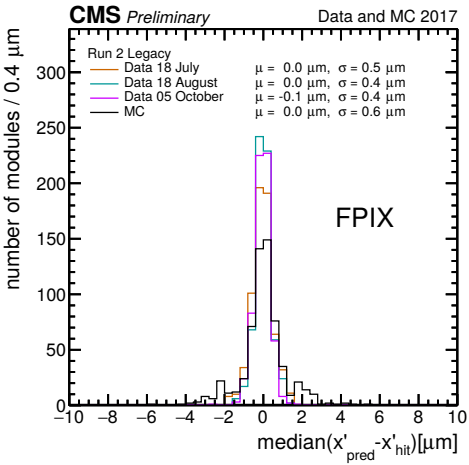

Distribution of median residuals in the local-x (x') coordinate for different components of the tracker system. The derived MC object (MC) is compared to three representative Data IOVs (18 July, 18 August, 5 October) to assess its validity as final geometry. The study corresponds to the MC scenario derived for 2017. The larger width of the MC distribution in the FPIX is driven by the systematic misalignment of 30 μm in the global z direction that was applied to the FPIX to achieve a better description of the data (see d_z vs. η plot).

Tracking

Selected IOV

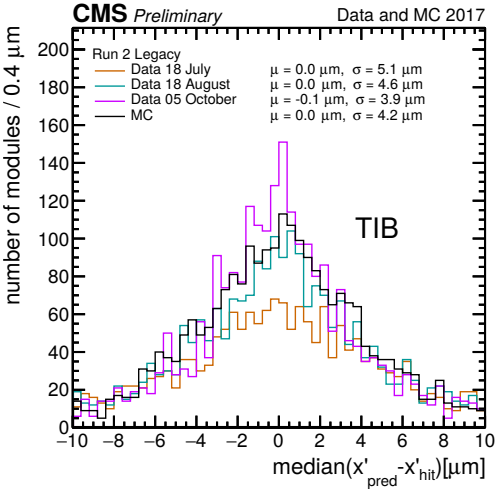

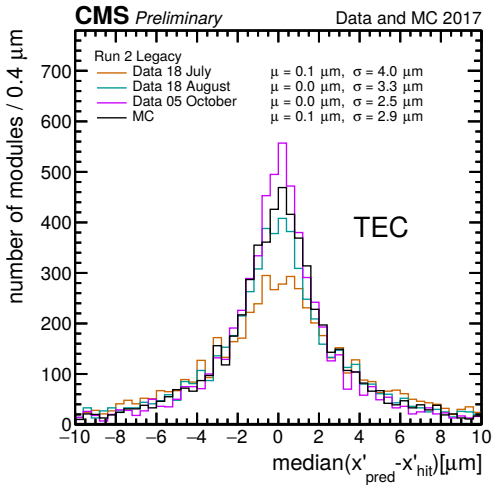

Distribution of median residuals in the local-x (x') coordinate for different components of the tracker system. The derived MC object (MC) is compared to three representative Data IOVs (18 July, 18 August, 5 October) to assess its validity as final geometry. The study corresponds to the MC scenario derived for 2017.

Tracking

Trends

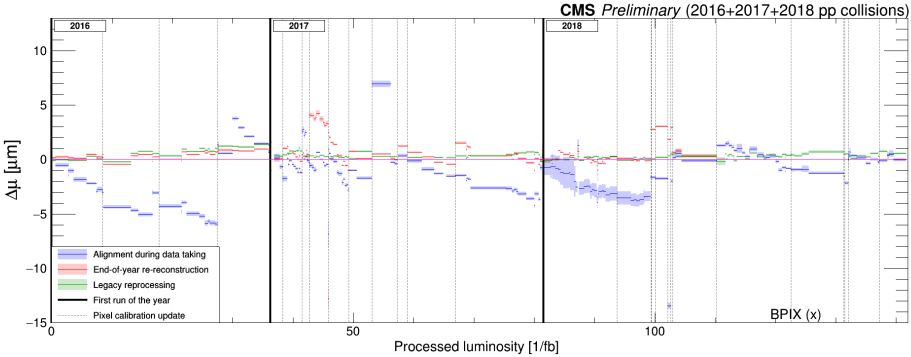

In the barrel region, DMR can be obtained separately for the modules with electric field pointing radially inwards or outwards. Difference of their mean values $\Delta\mu$ in the local-x (x') direction, which is orthogonal to the magnetic field, is an index of goodness in recovering Lorentz angle effects. Here, $\Delta\mu$ is shown for the pixel barrel modules as a function of integrated luminosity. The uncertainty corresponds to the square root of the quadratic sum of the uncertainties calculated separately for the inward and outward pointing modules. The vertical black solid lines indicate the first processed run for 2016, 2017, and 2018 data-taking period, respectively. The vertical dotted lines indicate a change in the tracker pixel calibration. The blue points correspond to the results with the alignment constants used during data-taking, the red points show the results with the alignment constants used during the 2016, 2017, and 2018 EOY re-reconstruction (notice there is no EOY re-reconstruction for the last $33\ \mathrm{fb}^{-1}$ of data-taking), the green points show the results with the alignment constants as obtained in the Run 2 Legacy alignment procedure. After the dedicated Run 2 Legacy alignment, the mean difference shows improved stability.

Tracking

Trends

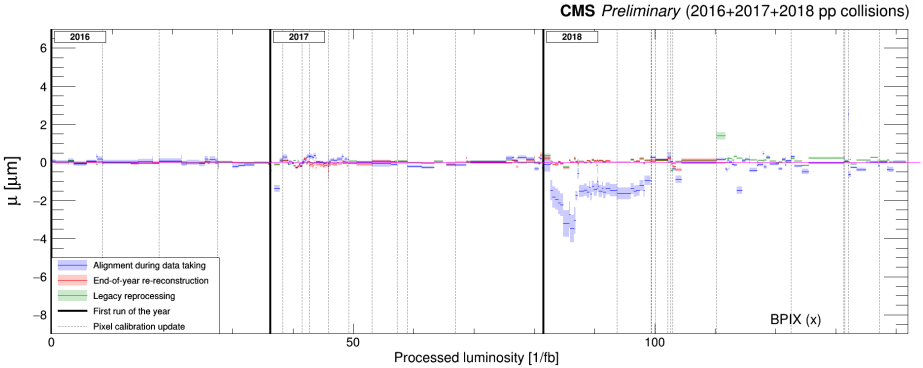

The mean value of the distribution of median residuals is plotted for the local-x (x') direction in the BPIX detector as a function of the integrated luminosity. The uncertainty corresponds to the standard mean error of the displayed quantity. The vertical black solid lines indicate the first processed run for 2016, 2017, and 2018 data-taking period, respectively. The vertical dotted lines indicate a change in the tracker pixel calibration. The blue points correspond to the results with the alignment constants used during data-taking, the red points show the results with the alignment constants used during the 2016, 2017, and 2018 EOY re-reconstruction (notice there is no EOY re-reconstruction for the last $33\ \mathrm{fb}^{-1}$ of data-taking), the green points show the results with the alignment constants as obtained in the Run 2 Legacy alignment procedure. After the dedicated Run 2 Legacy alignment, the mean value of the distribution of median residuals is shifted closer to zero.

Tracking

Trends

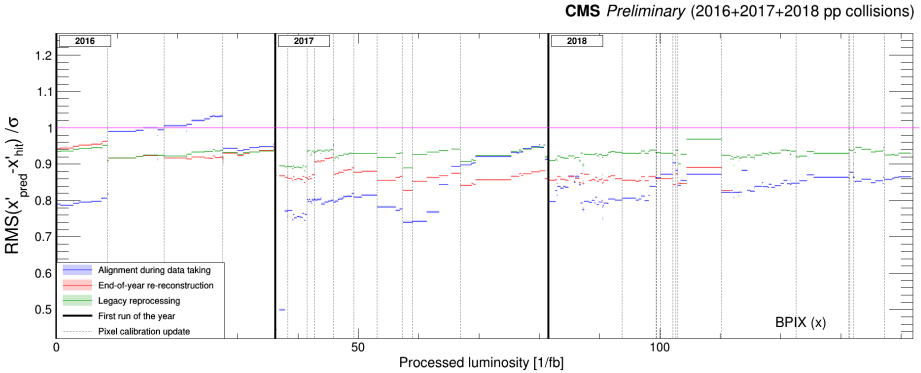

The RMS value of the distribution of normalized median residuals is plotted for the local-x (x') direction in the BPIX detector as a function of the integrated luminosity. The uncertainty corresponds to the standard deviation error of the displayed quantity. The vertical black solid lines indicate the first processed run for 2016, 2017 and 2018 data-taking period, respectively. The vertical dotted lines indicate a change in the tracker pixel calibration. The blue points correspond to the results with the alignment constants used during data-taking, the red points show the results with the alignment constants used during the 2016, 2017, and 2018 EOY re-reconstruction (notice there is no EOY re-reconstruction for the last $33\ \mathrm{fb}^{-1}$ of data-taking), the green points show the results with the alignment constants as obtained in the Run 2 Legacy alignment procedure. After the dedicated Run 2 Legacy alignment, pull goes closer to one.

Vertexing

Selected IOVs

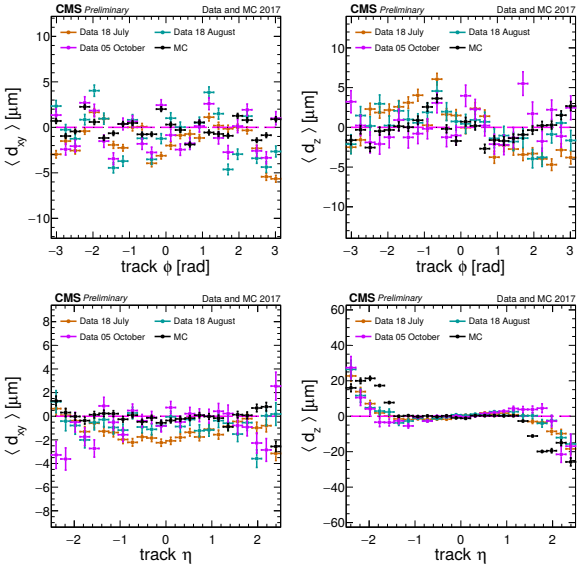

Distribution of mean impact parameter in the transverse plane d_{xy} and in the longitudinal plane d_z as a function of two angular variables ϕ and η. The derived MC object (MC) is compared to three representative Data IOVs (18 July, 18 August, 05 October) to assess its validity as final geometry. The study corresponds to the MC scenario derived for 2017. In the attempt of mimicking the observed behaviour in data in the $\langle d_z \rangle$ vs. η plot, a systematic misalignment of $30\ \mu\mathrm{m}$ in the global z-direction was applied to the FPIX endcaps.

Vertexing

Trends

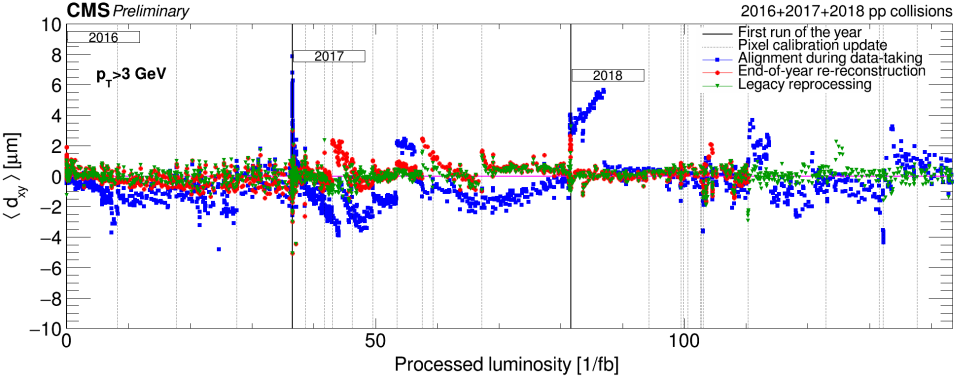

The mean of the average impact parameter in the transverse plane dxy as a function of processed luminosity. Only tracks with transverse momentum $p_T > 3\ \mathrm{GeV}$ are considered. The vertical black lines indicate the first processed run for 2016, 2017, and 2018 data-taking period, respectively. The vertical dotted lines indicate a change in the pixel tracker calibration. The blue points correspond to the results with the alignment constants used during data-taking, the red points to the 2016, 2017, and 2018 EOY re-reconstruction (notice there is no EOY re-reconstruction for the last $33\ \mathrm{fb}^{-1}$ of data-taking in 2018), and the green points to the results obtained in the Run 2 Legacy alignment procedure. During the LHC shutdown in winter 2016/17, the inner component (pixel detector) of the CMS tracking detector was replaced. The first few inverse picobarns of the 2017 pp collision run have been devoted to the commissioning of the new detector, resulting in sub-optimal tracking performance. This is visible in degraded impact parameter bias around the $36\ \mathrm{fb}^{-1}$ mark. Apart from this short period, aligning the tracker improves the mean of this distribution. Short IOVs with suboptimal configuration of the pixel local reconstruction (*e.g.* different high-voltage settings, inconsistent local reconstruction with alignment) can give rise to isolated peaks in the trends, especially during data taking. The suboptimal performance of the alignment during data taking at the beginning of 2018 is caused by the fact that the alignment was not updated by the PCL.

Vertexing

Trends

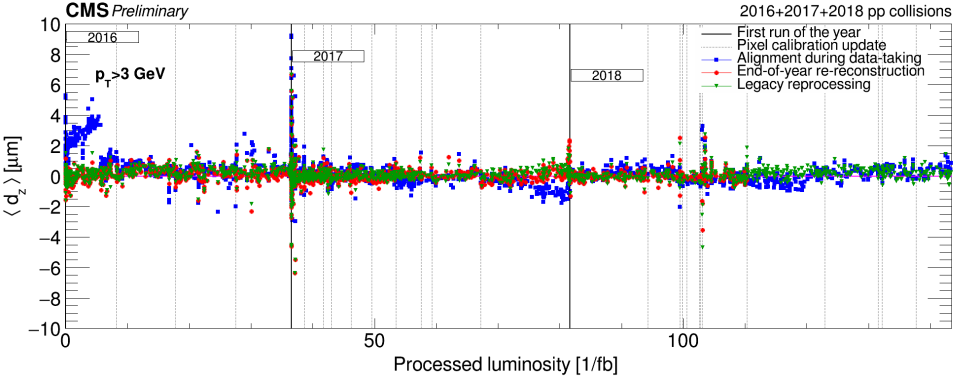

The mean of the average impact parameter in the longitudinal plane dz as a function of processed luminosity. Only tracks with transverse momentum $p_T > 3$ GeV are considered. The vertical black lines indicate the first processed run for 2016, 2017, and 2018 data-taking period, respectively. The vertical dotted lines indicate a change in the pixel tracker calibration. The blue points correspond to the results with the alignment constants used during data-taking, the red points to the 2016, 2017, and 2018 EOY re-reconstruction (notice there is no EOY re-reconstruction for the last 33 fb^{-1} of data-taking in 2018), and the green points to the results obtained in the Run 2 Legacy alignment procedure. During the LHC shutdown in winter 2016/17, the inner component (pixel detector) of the CMS tracking detector was replaced. The first few inverse picobarns of the 2017 pp collision run have been devoted to the commissioning of the new detector, resulting in sub-optimal tracking performance. This is visible in degraded impact parameter bias around the 36 fb^{-1} mark. Apart from this short period, aligning the tracker improves the mean of this distribution. Short IOVs with suboptimal configuration of the pixel local reconstruction (*e.g.* different high-voltage settings, inconsistent local reconstruction with alignment) can give rise to isolated peaks in the trends, especially during data taking. The suboptimal performance for the alignment during data taking at the beginning of 2016 is due to relative misalignment of the two half-barrels of the pixel detector along the z direction. This was not corrected by the alignment in the PCL, which was not active in that period.

Vertexing

Trends

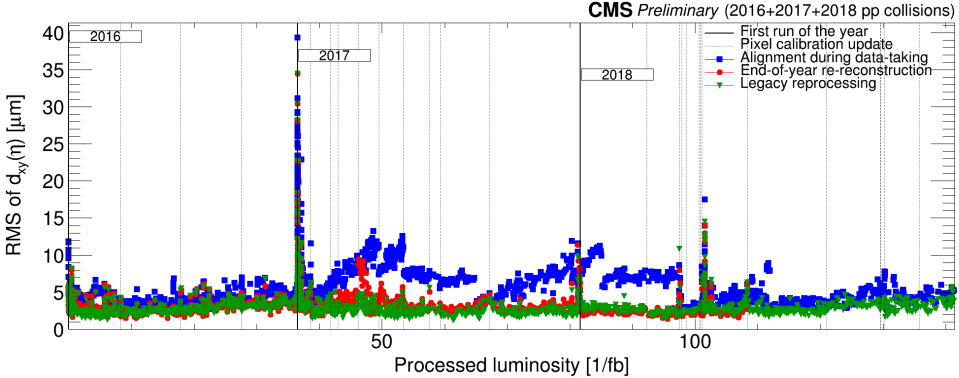

The RMS of the average impact parameter in the transverse plane dxy in bins of the track azimuth , as a function of processed luminosity. Only tracks with transverse momentum $p_T > 3\ \mathrm{GeV}$ are considered. The vertical black lines indicate the first processed run for 2016, 2017, and 2018 data-taking period, respectively. The vertical dotted lines indicate a change in the pixel tracker calibration. The blue points correspond to the results with the alignment constants used during data-taking, the red points to the 2016, 2017, and 2018 EOY re-reconstruction (notice there is no EOY re-reconstruction for the last $33\ \mathrm{fb}^{-1}$ of data-taking in 2018), and the green points to the results obtained in the Run 2 Legacy alignment procedure. During the LHC shutdown in winter 2016/17, the inner component (pixel detector) of the CMS tracking detector was replaced. The first few inverse picobarns of the 2017 pp collision run have been devoted to the commissioning of the new detector, resulting in sub-optimal tracking performance. This is visible in degraded impact parameter bias around the $36\ \mathrm{fb}^{-1}$ mark. Apart from this short period, aligning the tracker improves the mean of this distribution. Short IOVs with suboptimal configuration of the pixel local reconstruction (*e.g.* different high-voltage settings, inconsistent local reconstruction with alignment) can give rise to isolated peaks in the trends, especially during data taking. The suboptimal performance of the alignment during data taking at the beginning of 2018 is caused by the fact that the alignment was not updated by the PCL. The slopes for the alignment during data taking visible between two pixel calibration updates are due to radiation effects, causing rapid changes of the Lorentz drift. This effect can only be corrected by aligning with a finer granularity than the automated alignment implements.

Vertexing

Trends

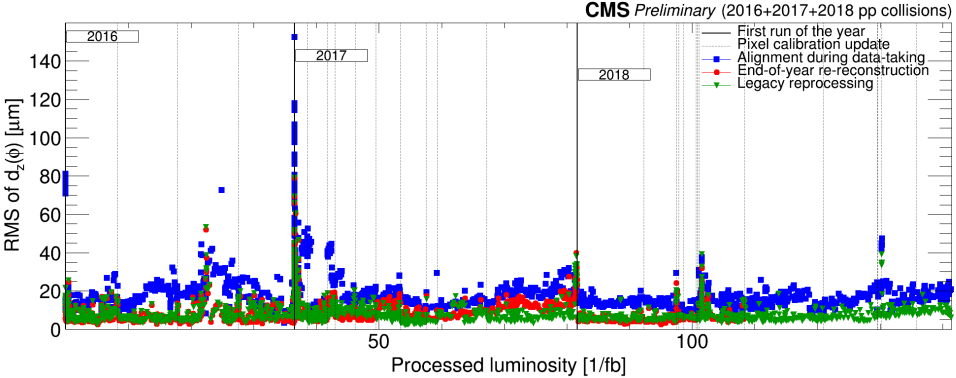

The RMS of the average impact parameter in the longitudinal plane dz in bins of the track azimuth , as a function of processed luminosity. Only tracks with transverse momentum $p_T > 3$ GeV are considered. The vertical black lines indicate the first processed run for 2016, 2017, and 2018 data-taking period, respectively. The vertical dotted lines indicate a change in the pixel tracker calibration. The blue points correspond to the results with the alignment constants used during data-taking, the red points to the 2016, 2017, and 2018 EOY re-reconstruction (notice there is no EOY re-reconstruction for the last $33\ \mathrm{fb}^{-1}$ of data-taking in 2018), and the green points to the results obtained in the Run 2 Legacy alignment procedure. During the LHC shutdown in winter 2016/17, the inner component (pixel detector) of the CMS tracking detector was replaced. The first few inverse picobarns of the 2017 pp collision run have been devoted to the commissioning of the new detector, resulting in sub-optimal tracking performance. This is visible in degraded impact parameter bias around the $36\ \mathrm{fb}^{-1}$ mark. Apart from this short period, aligning the tracker improves the mean of this distribution. Short IOVs with suboptimal configuration of the pixel local reconstruction (*e.g.* different high-voltage settings, inconsistent local reconstruction with alignment) can give rise to isolated peaks in the trends, especially during data taking.

Vertexing

Trends

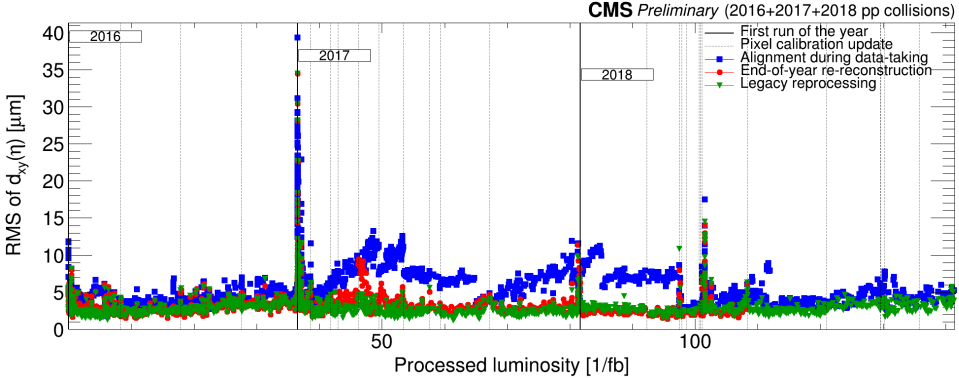

The RMS of the average impact parameter in the transverse plane dxy in bins of the track pseudorapidity η, as a function of processed luminosity. Only tracks with transverse momentum $p_T > 3\ \mathrm{GeV}$ are considered. The vertical black lines indicate the first processed run of the 2016, 2017, and 2018 data-taking period, respectively. The vertical dotted lines indicate a change in the pixel tracker calibration. The blue points correspond to the results with the alignment constants used during data-taking, the red points to the 2016, 2017, and 2018 EOY re-reconstruction (notice there is no EOY re-reconstruction for the last $33\ \mathrm{fb}^{-1}$ of data-taking in 2018), and the green points to the results obtained in the Run 2 Legacy alignment procedure. During the LHC shutdown in winter 2016/17, the inner component (pixel detector) of the CMS tracking detector was replaced. The first few inverse picobarns of the 2017 pp collision run have been devoted to the commissioning of the new detector, resulting in sub-optimal tracking performance. This is visible in degraded impact parameter bias around the $36\ \mathrm{fb}^{-1}$ mark. Apart from this short period, aligning the tracker improves the mean of this distribution. Short IOVs with suboptimal configuration of the pixel local reconstruction (*e.g.* different high-voltage settings, inconsistent local reconstruction with alignment) can give rise to isolated peaks in the trends, especially during data taking.

Vertexing

Trends

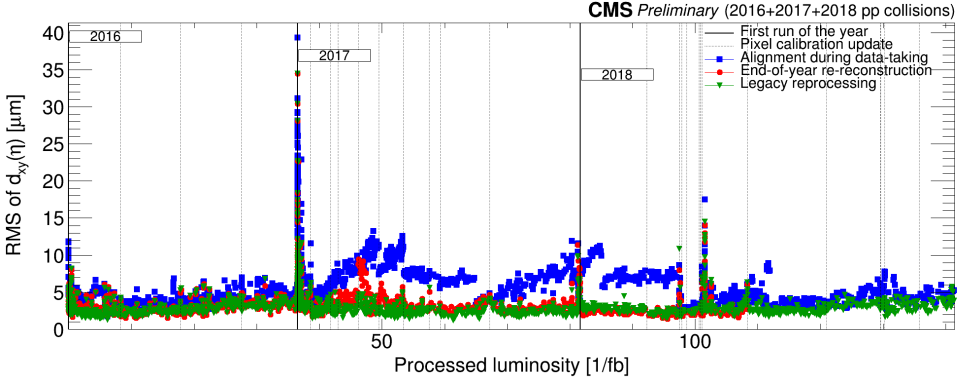

The RMS of the average impact parameter in the longitudinal plane dz in bins of the track pseudorapidity η, as a function of processed luminosity. Only tracks with transverse momentum $p_T > 3\ \mathrm{GeV}$ are considered. The vertical black lines indicate the first processed run of the 2016, 2017, and 2018 data-taking period, respectively. The vertical dotted lines indicate a change in the pixel tracker calibration. The blue points correspond to the results with the alignment constants used during data-taking, the red points to the 2016, 2017, and 2018 EOY re-reconstruction (notice there is no EOY re-reconstruction for the last $33\ \mathrm{fb}^{-1}$ of data-taking in 2018), and the green points to the results obtained in the Run 2 Legacy alignment procedure. During the LHC shutdown in winter 2016/17, the inner component (pixel detector) of the CMS tracking detector was replaced. The first few inverse picobarns of the 2017 pp collision run have been devoted to the commissioning of the new detector, resulting in sub-optimal tracking performance. This is visible in degraded impact parameter bias around the $36\ \mathrm{fb}^{-1}$ mark. Apart from this short period, aligning the tracker improves the mean of this distribution. Short IOVs with suboptimal configuration of the pixel local reconstruction (*e.g.* different high-voltage settings, inconsistent local reconstruction with alignment) can give rise to isolated peaks in the trends, especially during data taking.

Tracking of cosmic rays

Selected IOVs

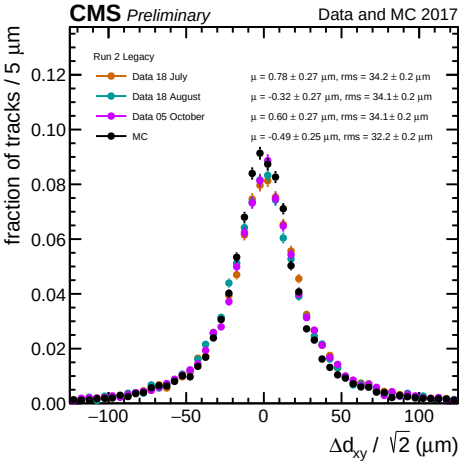

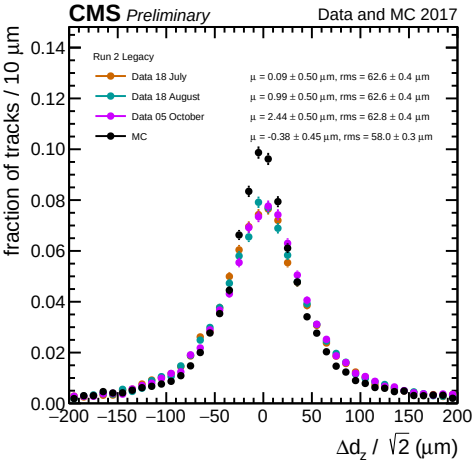

Difference in impact parameter in the longitudinal and transverse plane between two halves of cosmic tracks. The derived MC object (MC) is compared to three representative Data IOVs (18 July, 18 August, 05 October) to assess its validity as final geometry. The study corresponds to the MC scenario derived for 2017.

Tracking of cosmic rays

Average

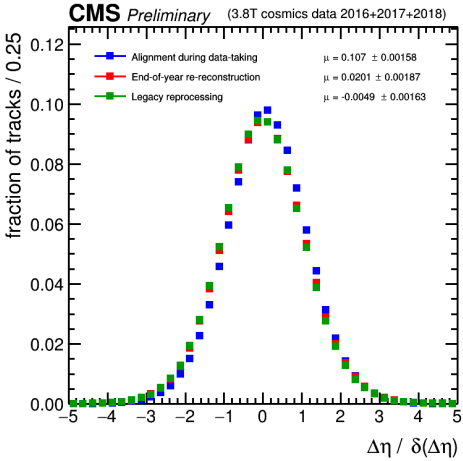

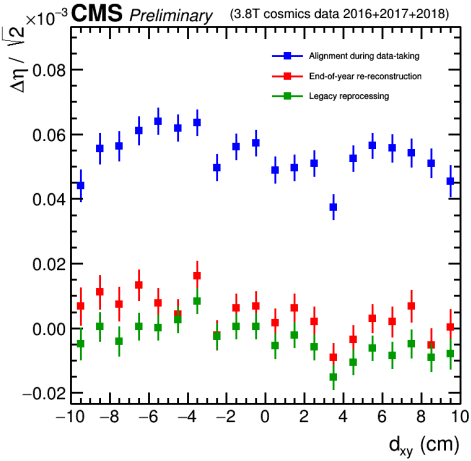

Pull of the normalised difference in the track pseudorapidity η (left) and the normalised difference in the track pseudorapidity η, in bins of the transverse impact parameter d_{xy} (right), between the two halves of cosmic tracks recorded with the CMS magnet at 3.8 T during 2016, 2017, and 2018 period, split at the point of the closest approach to the interaction region. Comparison is made for the results with the alignment constants used during data-taking (blue points), the alignment constants used during the 2016, 2017, and 2018 EOY re-reconstruction (red points) and the alignment constants as obtained in the Run 2 Legacy alignment procedure (green points). Aligning the tracker under the Run 2 Legacy alignment procedure shows better performance.

Di-muon

Selected IOV

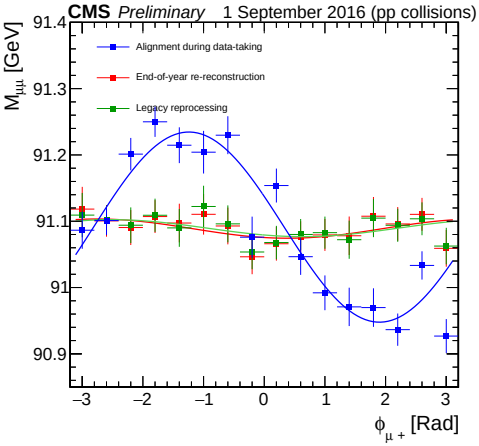

Plot of Z mass vs the azimuth angle (ϕ) of the positive μ_+. As a representative example, run from 01 September 2016 was selected. The blue points correspond to the results with the alignment constants used during data-taking, the red points show the results with the alignment constants used during the 2016, 2017, and 2018 EOY re-reconstruction, the green points show the results with the alignment constants as obtained in the Run 2 Legacy alignment procedure. The fitted lines are obtained by fitting Z Mass vs the azimuth angle (ϕ) to a function of the form $Acos(\phi + \phi_0) + b$. Any systematic distortion over some periodic boundary is expected to also be periodic, which motivates our fit. This can be interpreted as the first Fourier mode of the function that parameterizes our distortion.

Di-muon

Selected IOV

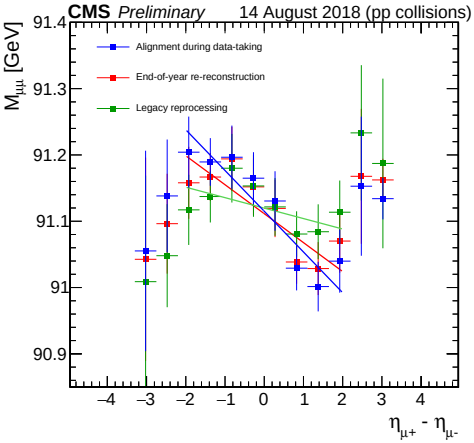

Plot of Z mass vs $\Delta\eta_{\mu\mu}$. As a representative example, run from 14 August 2018 was selected. The blue points correspond to the results with the alignment constants used during data-taking, the red points show the results with the alignment constants used during the 2016, 2017, and 2018 EOY re-reconstruction, the green points show the results with the alignment constants as obtained in the Run 2 Legacy alignment procedure. The fitted lines are obtained by fitting Z mass vs $\Delta\eta_{\mu\mu}$ to function of the form $\epsilon\Delta\eta_{\mu\mu} + b$. Fit is only considered from -2 to 2 due to nonlinear behavior outside of this range.

Di-muon

Average

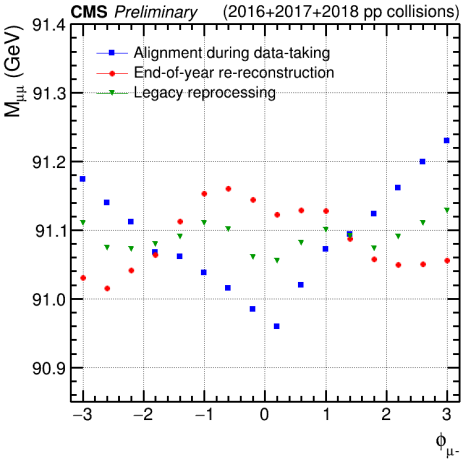

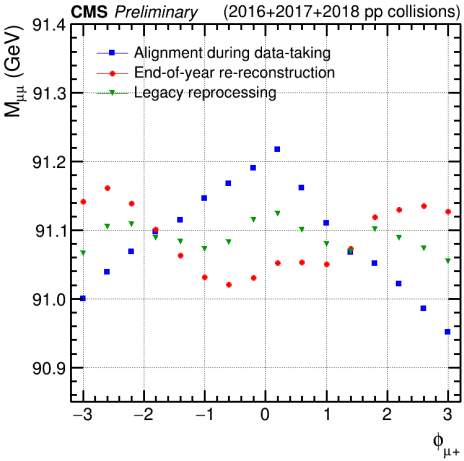

Reconstructed $Z \rightarrow \mu\mu$ mass as a function of the azimuth angle ϕ of the negatively charged muon (left) and the positively charged muon (right), respectively. The blue points correspond to the results with the alignment constants used during data-taking, the red points show the results with the alignment constants used during the 2016, 2017, and 2018 EOY re-reconstruction, the green points show the results with the alignment constants as obtained in the Run 2 Legacy alignment procedure. Aligning the tracker under Run 2 Legacy alignment procedure showed an improvement to the uniformity of the reconstructed $Z \rightarrow \mu\mu$ mass.

Di-muon

Average

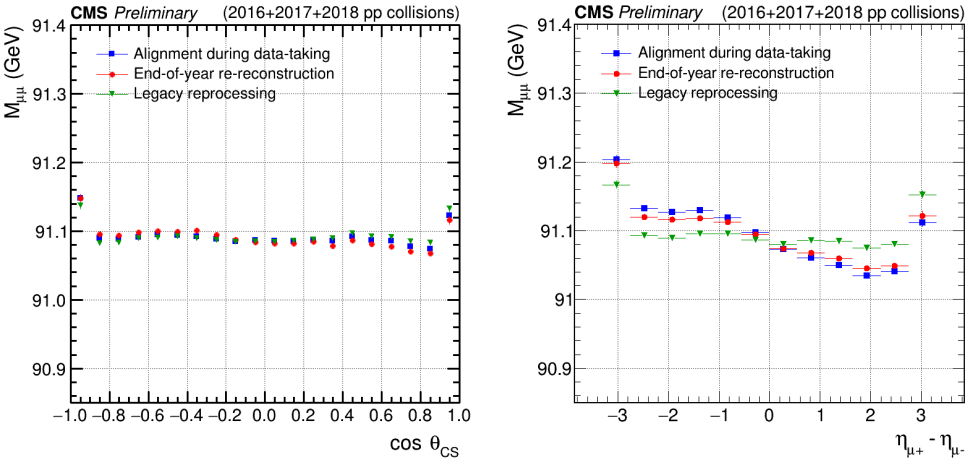

Reconstructed $Z \to \mu\mu$ mass as a function of difference in η between the positively and negatively charged muons (left) and as a function of the angle $\cos(\theta_{\mathrm{CS}})$ in the Collins-Sooper frame of the reconstructed Z boson (right). The blue points correspond to the results with the alignment constants used during data-taking, the red points show the results with the alignment constants used during the 2016, 2017, and 2018 EOY re-reconstruction, the green points show the results with the alignment constants as obtained in the Run 2 Legacy alignment procedure. Aligning the tracker under Run 2 Legacy alignment procedure showed an improvement to the uniformity of the reconstructed $Z \to \mu\mu$ mass.

Di-muon

Trends

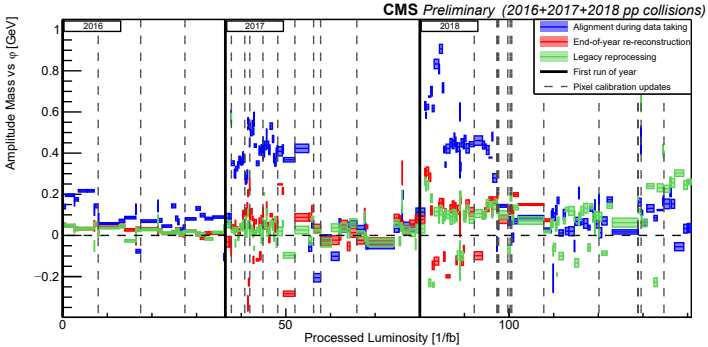

The Amplitude (A) given by fitting Z Mass vs the azimuth angle(ϕ) of the positive μ_+ track to a function of the form $Acos(\phi + \phi_0) + b$ as a function of processed luminosity. This Amplitude shows the average spread of the Z-mass with respects to $\phi\mu_+$, which is expected to be zero in a well-aligned detector. A non-zero Amplitude indicates that reconstructed mass has some dependence on the spatial coordinates of the detector. We observe significant improvement between Legacy Reprocessing and other alignment campaigns. Error bars correspond to the uncertainty on fitting parameters calculated by χ^2 regression. The vertical black solid lines indicate the first processed run for 2016, 2017, and 2018 data-taking period, respectively. The vertical dotted lines indicate a change in the pixel tracker calibration. The blue bands correspond to the results with the alignment constants used during data-taking, the red bands show the results with the alignment constants used during the 2016, 2017, and 2018 EOY re-reconstruction (notice there is no EOY re-reconstruction for the last $33\ \mathrm{fb}^{-1}$ of data-taking), the green bands show the results with the alignment constants as obtained in the Run 2 Legacy alignment procedure. During the LHC shutdown in winter 2016/17, the pixel detector was replaced.

Di-muon

Trends

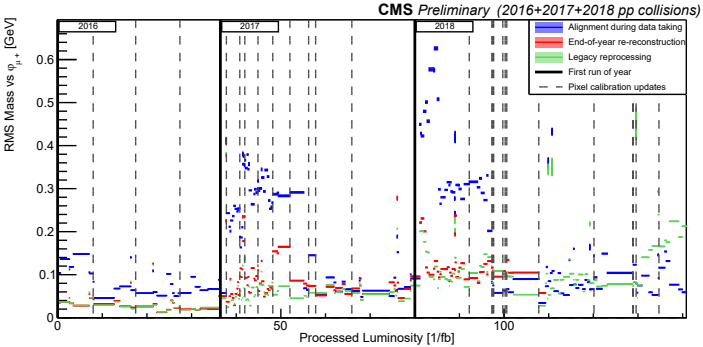

The RMS of Z masses binned over ϕ_{μ_+} as a function of processed luminosity. The RMS a good measure of the spread of the Z-mass with respect to $\phi\mu_+$, which is expected to be zero in a well-aligned detector. A non-zero RMS indicates that reconstructed mass has some dependence on the spatial coordinates of the detector. We observe significant improvement between Legacy Reprocessing and other alignment campaigns. The vertical black solid lines indicate the first processed run for 2016, 2017, and 2018 data-taking period, respectively. The vertical dotted lines indicate a change in the pixel tracker calibration. The blue bands correspond to the results with the alignment constants used during data-taking, the red bands show the results with the alignment constants used during the 2016, 2017, and 2018 EOY re-reconstruction (notice there is no EOY re-reconstruction for the last $33\ \mathrm{fb}^{-1}$ of data-taking), the green bands show the results with the alignment constants as obtained in the Run 2 Legacy alignment procedure. During the LHC shutdown in winter 2016/17, the pixel detector was replaced.

Di-muon

Trends

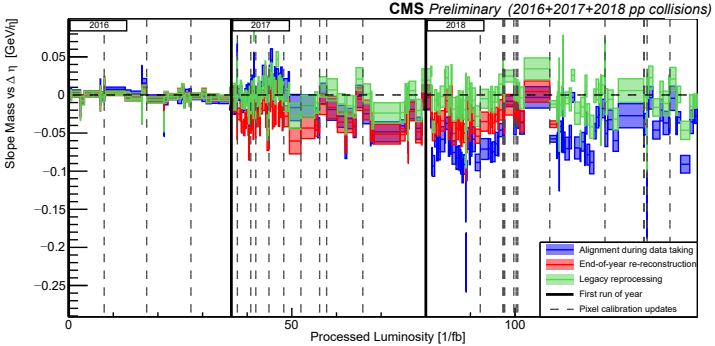

The slope (ϵ) given by fitting Z mass vs $\Delta\eta_{\mu\mu}$ of the two muons to a linear function of the form $\epsilon\Delta\eta_{\mu\mu} + b$ as a function of processed luminosity. In an ideal alignment we expect that reconstructed mass has no dependence on the pseudo-rapidities of decay products between -2 and 2. At these pseudo-rapidities, particles travel through most of the active area of the Barrel Pixel. We observe significant improvement between Legacy Reprocessing and other alignment campaigns. The vertical black solid lines indicate the first processed run for 2016, 2017, and 2018 data-taking period, respectively. The vertical dotted lines indicate a change in the pixel tracker calibration. The blue bands correspond to the results with the alignment constants used during data-taking, the red bands show the results with the alignment constants used during the 2016, 2017, and 2018 EOY re-reconstruction (notice there is no EOY re-reconstruction for the last $33\ \mathrm{fb}^{-1}$ of data-taking), the green bands show the results with the alignment constants as obtained in the Run 2 Legacy alignment procedure. During the LHC shutdown in winter 2016/17, the pixel detector was replaced.

Barycentre

Trends

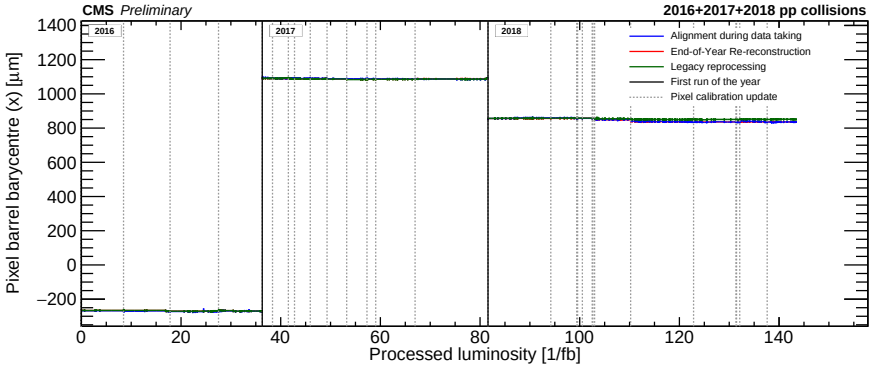

Barycentre position of the BPIX detector as a function of the integrated luminosity, determined as the centre-of-gravity of BPIX modules only. The vertical black solid lines indicate the first processed run of the 2016, 2017, and 2018 data-taking period, respectively. The vertical dotted lines indicate changes in the pixel calibration. The blue line corresponds to the results with the alignment constants used during data taking, the red line corresponds to the results with alignment constants during the 2016, 2017, and 2018 End-of-year (EOY) re-reconstruction (notice there is no EOY re-reconstruction for the last $33\ \mathrm{fb}^{-1}$ of data-taking in 2018), the green line corresponds to the results with alignment constants as obtained in the Run 2 Legacy alignment procedures. Large position differences at the beginning of 2017 and 2018 data taking periods are caused by the fact that the pixel detector was extracted during the shutdowns and then re-installed, in occasion of the Phase-1 upgrade in 2017, and for module replacements in 2018.

Barycentre

Trends

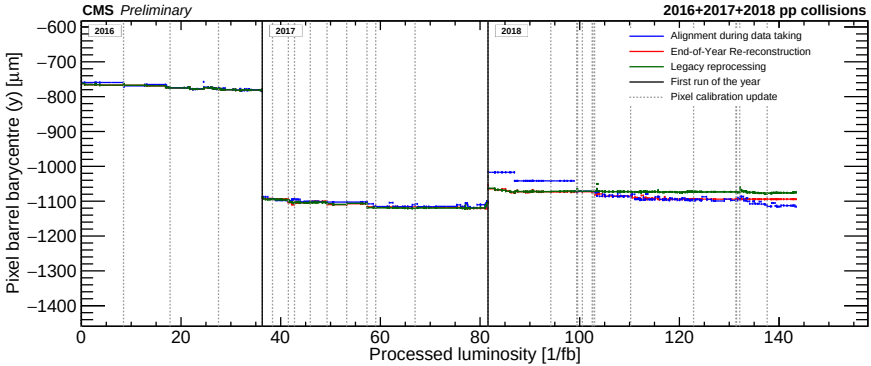

Barycentre position of the BPIX detector as a function of the integrated luminosity, determined as the centre-of-gravity of BPIX modules only. The vertical black solid lines indicate the first processed run of the 2016, 2017, and 2018 data-taking period, respectively. The vertical dotted lines indicate changes in the pixel calibration. The blue line corresponds to the results with the alignment constants used during data taking, the red line corresponds to the results with alignment constants during the 2016, 2017, and 2018 End-of-year (EOY) re-reconstruction (notice there is no EOY re-reconstruction for the last $33\ \mathrm{fb}^{-1}$ of data-taking in 2018), the green line corresponds to the results with alignment constants as obtained in the Run 2 Legacy alignment procedures. Large position differences at the beginning of 2017 and 2018 data taking periods are caused by the fact that the pixel detector was extracted during the shutdowns and then re-installed, in occasion of the Phase-1 upgrade in 2017, and for module replacements in 2018.

Overlap

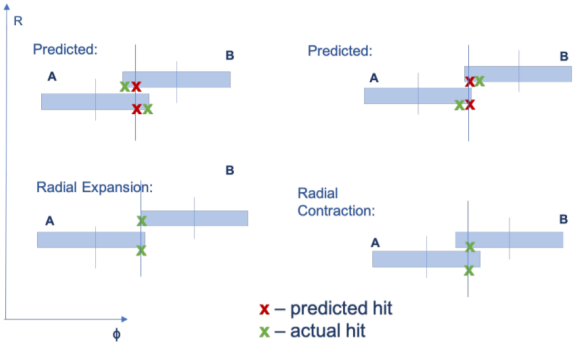

Diagram demonstrating a shift in ϕ coordinate of predicted hits for modules overlapping in the ϕ direction of the tracker. An overlap in any direction is defined as any track with hits in two consecutive modules in the same layer of the detector. In this diagram, module A and module B are in the same layer of the tracker and have hits from the same track. Modules only differ in their ϕ coordinate so we say these modules are overlapping in the phi direction. We show effects under both radial expansion and contraction. Also note that shift of the effective charge collection location on the module can also cause of shifts in measured hit location

Overlap

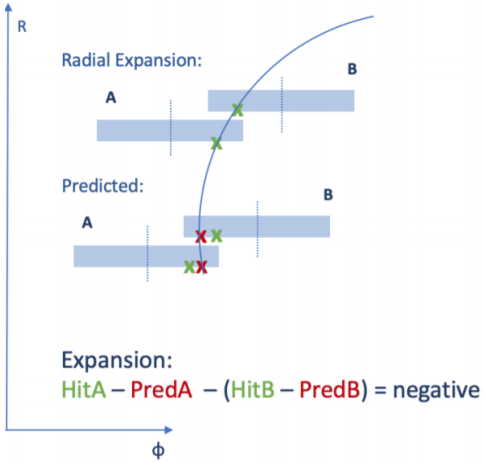

Diagram demonstrating the effect of radial expansion on measured ϕ coordinate for modules overlapping in the ϕ direction of the tracker. The definition of measured difference in a measured hit and predicted hit is given as well. This quantity would be defined as $(\Delta\delta_\phi)_\phi$ or the difference in ϕ residuals for modules overlapping in the ϕ direction in the tracker.

Overlap

Selected IOV

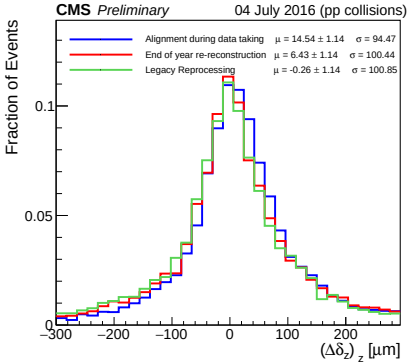

Distribution of difference in z residuals for modules overlapping in the z direction for the Barrel Pixel of the tracker ($(\Delta\delta_z)_z$). As a representative example, run from 04 July 2016 was selected. The blue line corresponds to the results with the alignment constants used during data-taking, the red lines show the results with the alignment constants used during the 2016, 2017, and 2018 EOY re-reconstruction, the green lines show the results with the alignment constants as obtained in the Run 2 Legacy alignment procedure. The quoted means μ and standard deviations σ are the parameters of a Gaussian fit to the distributions.

Overlap

Selected IOV

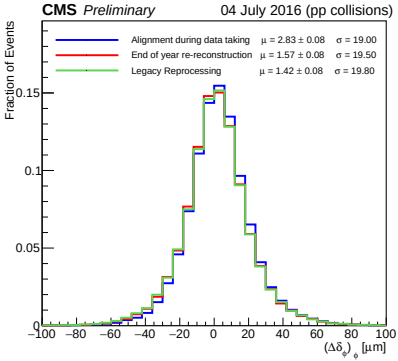

Distribution of difference in ϕ residuals for modules overlapping in the ϕ direction for the Barrel Pixel of the tracker ($(\Delta\delta_\phi)_\phi$). As a representative example, run from 04 July 2016 was selected. The blue line corresponds to the results with the alignment constants used during data-taking, the red lines show the results with the alignment constants used during the 2016, 2017, and 2018 EOY re-reconstruction, the green lines show the results with the alignment constants as obtained in the Run 2 Legacy alignment procedure. The quoted means μ and standard deviations σ are the parameters of a Gaussian fit to the distributions.

Overlap

Selected IOV

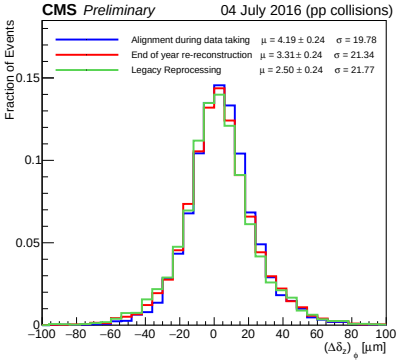

Distribution of difference in ϕ residuals for modules overlapping in the z direction for the Barrel Pixel of the tracker ($(\Delta\delta_\phi)_z$). As an example, run from 04 July 2016 was selected. The blue line corresponds to the results with the alignment constants used during data-taking, the red lines show the results with the alignment constants used during the 2016, 2017, and 2018 EOY re-reconstruction, the green lines show the results with the alignment constants as obtained in the Run 2 Legacy alignment procedure. The quoted means μ and standard deviations σ are the parameters of a Gaussian fit to the distributions

Overlap

Selected IOV

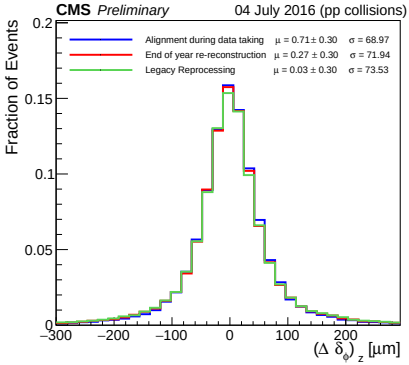

Distribution of difference in z residuals for modules overlapping in the ϕ direction for the Barrel Pixel of the tracker ($\Delta_z \delta_\phi$). As an example, run from 04 July 2016 was selected. The blue line corresponds to the results with the alignment constants used during data-taking, the red lines show the results with the alignment constants used during the 2016, 2017, and 2018 EOY re-reconstruction, the lines show the results with the alignment constants as obtained in the Run 2 Legacy alignment procedure. The quoted means μ and standard deviations σ are the parameters of a Gaussian fit to the distributions.

Overlap

Trends

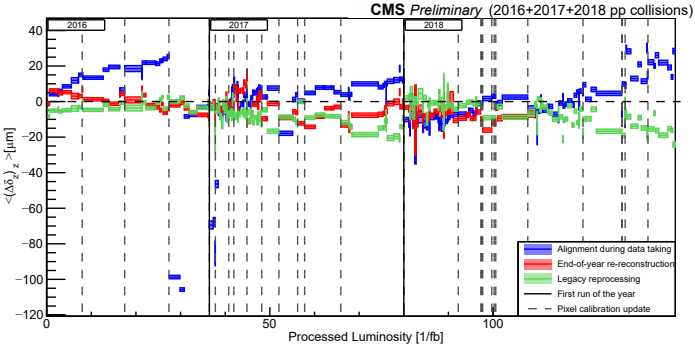

The mean difference in z residuals for modules overlapping in the z direction in the Barrel Pixel ($(\Delta\delta_z)_z$), as a function of processed luminosity. The non-zero value of the mean difference of residuals could be explained either by the geometrical shift of the modules, such as expansion of the detector along the z axis, or by the shift of the effective charge collection location, such as imperfect recovering of the Lorentz angle effects. The vertical black solid lines indicate the first processed run for 2016, 2017, and 2018 data-taking period, respectively. The vertical dotted lines indicate a change in the pixel tracker calibration. The blue bands correspond to the results with the alignment constants used during data-taking, the red bands show the results with the alignment constants used during the 2016, 2017, and 2018 EOY re-reconstruction (notice there is no EOY re-reconstruction for the last $33\ \mathrm{fb}^{-1}$ of data-taking), the green bands show the results with the alignment constants as obtained in the Run 2 Legacy alignment procedure. There is an improvement of End-of-year and Legacy Reprocessing over Alignment during data taking. During the LHC shutdown in winter 2016/17, the pixel detector was replaced.

Overlap

Trends

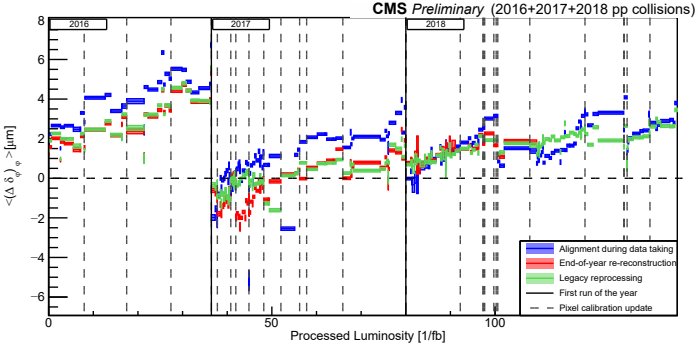

The mean difference in ϕ residuals for modules overlapping in the ϕ direction in the Barrel Pixel ($(\Delta\delta_\phi)_\phi$), as a function of processed luminosity. The vertical black solid lines indicate the first processed run for 2016, 2017, and 2018 data-taking period, respectively. The non-zero value of the mean difference of residuals could be explained either by the geometrical shift of the modules, such as expansion of the detector along the r axis, or by the shift of the effective charge collection location. The vertical dotted lines indicate a change in the pixel tracker calibration. The blue bands correspond to the results with the alignment constants used during data-taking, the red bands show the results with the alignment constants used during the 2016, 2017, and 2018 EOY re-reconstruction (notice there is no EOY re-reconstruction for the last $33\ \mathrm{fb}^{-1}$ of data-taking), the green bands show the results with the alignment constants as obtained in the Run 2 Legacy alignment procedure. There is an improvement of End-of-year and Legacy Reprocessing over Alignment during data taking. During the LHC shutdown in winter 2016/17, the pixel detector was replaced.

Overlap

Trends

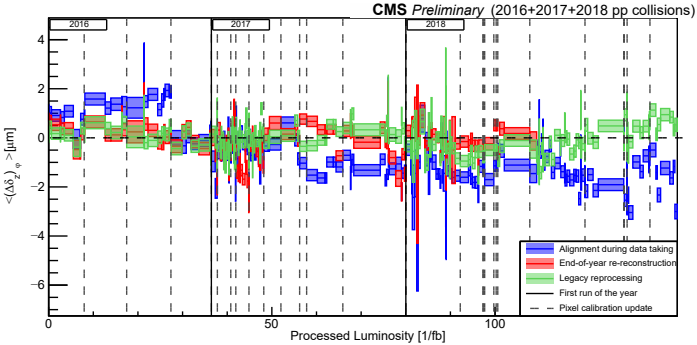

The mean difference in ϕ residuals for modules overlapping in the z direction in the Barrel Pixel $((\Delta\delta_\phi)_z)$, as a function of processed luminosity. The non-zero value of the mean difference of residuals could be explained either by the geometrical shift of the modules or by the shift of the effective charge collection location. The vertical black solid lines indicate the first processed run for 2016, 2017, and 2018 data-taking period, respectively. The vertical dotted lines indicate a change in the pixel tracker calibration. The blue bands correspond to the results with the alignment constants used during data-taking, the red bands show the results with the alignment constants used during the 2016, 2017, and 2018 EOY re-reconstruction (notice there is no EOY re-reconstruction for the last $33\ \mathrm{fb}^{-1}$ of data-taking), the green bands show the results with the alignment constants as obtained in the Run 2 Legacy alignment procedure. There is an improvement of End-of-year and Legacy Reprocessing over Alignment during data taking. During the LHC shutdown in winter 2016/17, the pixel detector was replaced.

Overlap

Trends

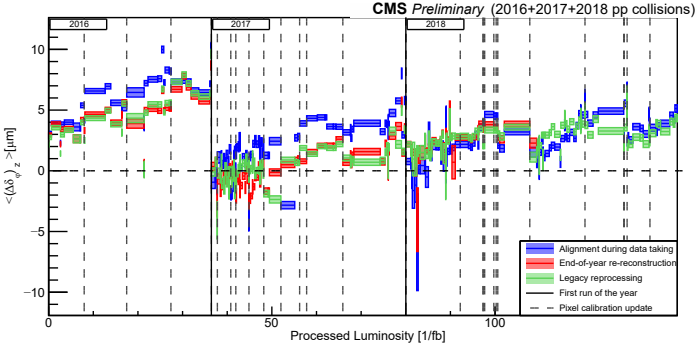

The mean difference in z residuals for modules overlapping in the ϕ direction in the Barrel Pixel $(\Delta\delta_z)_\phi$) , as a function of processed luminosity. The non-zero value of the mean difference of residuals could be explained either by the geometrical shift of the modules or by the shift of the effective charge collection location. The vertical black solid lines indicate the first processed run for 2016, 2017, and 2018 data-taking period, respectively. The vertical dotted lines indicate a change in the pixel tracker calibration. The blue bands correspond to the results with the alignment constants used during data-taking, the red bands show the results with the alignment constants used during the 2016, 2017, and 2018 EOY re-reconstruction (notice there is no EOY re-reconstruction for the last $33\ \mathrm{fb}^{-1}$ of data-taking), the green bands show the results with the alignment constants as obtained in the Run 2 Legacy alignment procedure. There is an improvement of End-of-year and Legacy Reprocessing over Alignment during data taking. During the LHC shutdown in winter 2016/17, the pixel detector was replaced.

Uncertainties

- Normalized hit residual distributions $(x_{trk} - x_{hit})/\sigma$, where σ is the quadratic sum of the cluster position estimation (CPE) error and the track uncertainty, should have the same width as design MC simulation
- misalignment broadens the hit residual distribution
- introduce additional uncertainty such that the total residual uncertainty is given by: $\sigma_r^2 = \sigma^2 + \sigma_{\text{align}}^2$
- if σ_{align} correctly estimated: $(x_{trk} - x_{hit})/\sigma_r$ has a width of unity, assuming the CPE error is estimated correctly

$\longrightarrow$ APEs needed for χ^2/ndf determination of track candidates, included in the tracking covariance matrix and crucial for the hit association windows used in pattern recognition

Uncertainties

Selected IOV

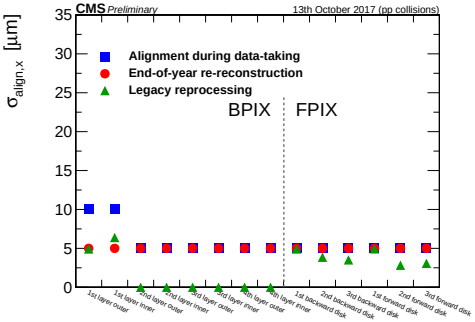

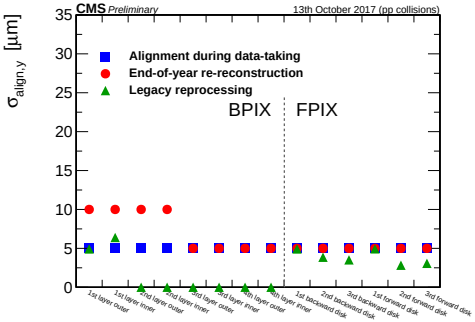

The contribution from the misalignment of the sensors to the total hit resolution is shown for the tracker pixel detector and split into module categories that characterize the hierarchical structure of each substructure. As an example, a data sample recorded in October 2017 was selected as a representative sample showing the performance for the detector geometry present in 2017 and 2018. The blue points correspond to the results with the alignment constants used during data-taking, the red points show the results with the alignment constants used during 2017 EOY re-reconstruction, the green points show the results with the alignment constants as obtained in the Run 2 Legacy alignment procedure. The results added in quadrature with the local cluster position estimation (CPE) error yield the hit resolution, therefore the true alignment precision of a module may be different depending on the local CPE error. The values are zero, if the measurement accuracy is at least as good as the design values. The results obtained from the Legacy reprocessing are more granular and yield smaller or similar alignment errors than the alignment errors obtained during data-taking or from the EOY re-reconstruction in most module categories.

Uncertainties

Selected IOV

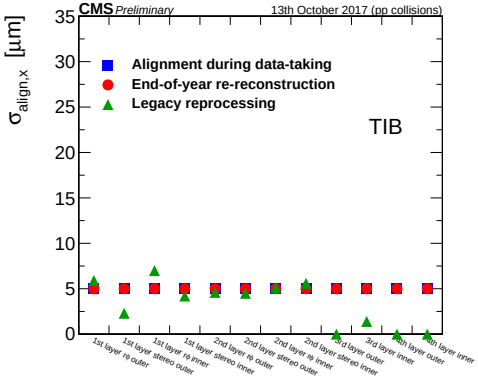

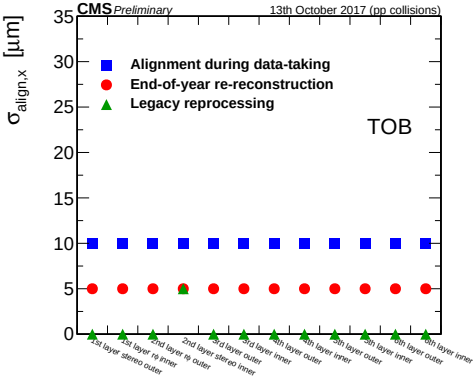

The contribution from the misalignment of the sensors to the total hit resolution is shown for the barrel region of the strip detector and split into module categories that characterize the hierarchical structure of each substructure. As an example, a data sample recorded in October 2017 was selected as a representative sample showing the performance for the detector geometry present in 2017 and 2018. The blue points correspond to the results with the alignment constants used during data-taking, the red points show the results with the alignment constants used during 2017 EOY re-reconstruction, the green points show the results with the alignment constants as obtained in the Run 2 Legacy alignment procedure. The results added in quadrature with the local cluster position estimation (CPE) error yield the hit resolution, therefore the true alignment precision of a module may be different depending on the local CPE error. The values are zero, if the measurement accuracy is at least as good as the design values. The results obtained from the Legacy reprocessing are more granular and yield smaller or similar alignment errors than the alignment errors obtained during data-taking or from the EOY re-reconstruction in most module categories.

Uncertainties

Selected IOV

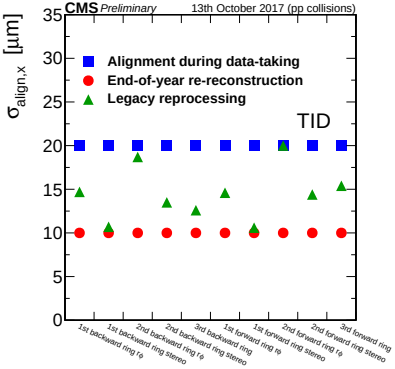

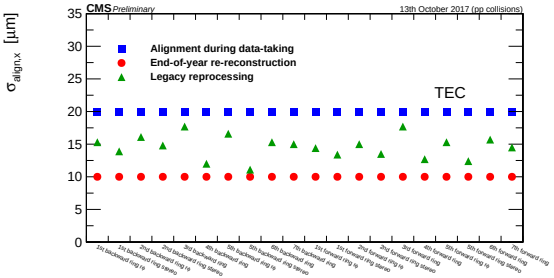

The contribution from the misalignment of the sensors to the total hit resolution is shown for the end-cap regions of the strip detector and split into module categories that characterize the hierarchical structure of each substructure. As an example, a data sample recorded in October 2017 was selected as a representative sample showing the performance for the detector geometry present in 2017 and 2018. The blue points correspond

Uncertainties

Trends

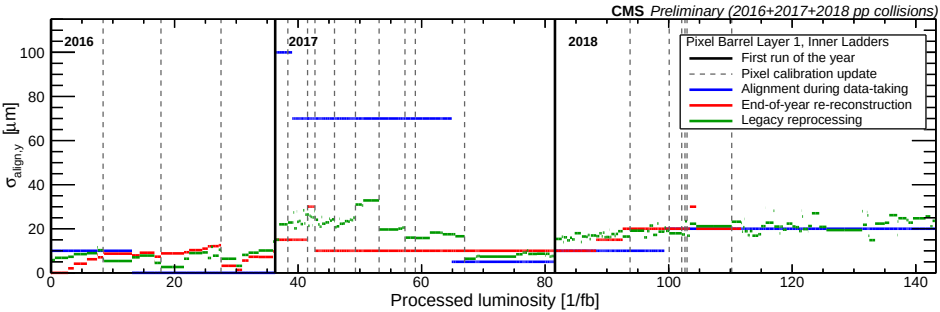

The contribution from the misalignment of the sensors to the total hit resolution for the inner ladders of the first pixel layer in local y-direction is shown for the Run 2 data-taking from 2016 to 2018 in dependency of the cumulative integrated luminosity. Shown are the results for the prompt reconstruction (blue), the end-of-year (EOY) re-reconstruction (red, notice there is no EOY re-reconstruction for the last $33\ \mathrm{fb}^{-1}$ of data-taking), and the legacy reprocessing (green). The vertical dashed lines indicate updates of the pixel calibration. The alignment error mainly varies between 0 and $30\ \mu\mathrm{m}$ and is only larger for the prompt-reconstruction at the beginning of the data-taking period in 2017, because the inner component (pixel detector) of the CMS tracking detector was replaced. For the legacy reprocessing, measurements were performed with higher granularity. Legacy measurements might have larger values compared to earlier reconstructions due to the higher granularity and because a decrease of the cluster position estimation error can result in an increase of the alignment position error. The values are zero, if the measurement accuracy is at least as good as the design values.

Uncertainties

Trends

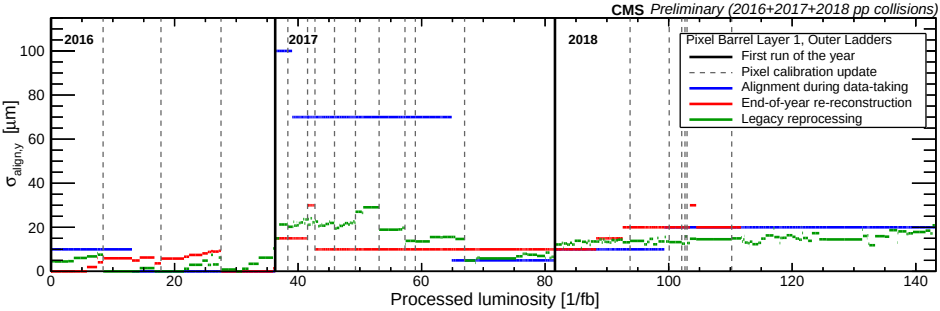

The contribution from the misalignment of the sensors to the total hit resolution for the outer ladders of the first pixel layer in local y-direction is shown for the Run 2 data-taking from 2016 to 2018 in dependency of the cumulative integrated luminosity. Shown are the results for the prompt reconstruction (blue), the end-of-year (EOY) re-reconstruction (red, notice there is no EOY re-reconstruction for the last $33\ \mathrm{fb}^{-1}$ of data-taking), and the legacy reprocessing (green). The vertical dashed lines indicate updates of the pixel calibration. The alignment error mainly varies between 0 and 30 mum and is only larger for the prompt-reconstruction at the beginning of the data-taking period in 2017, because the inner component (pixel detector) of the CMS tracking detector was replaced. The resolution of the outer ladders is better compared to the inner ladders due to the higher radiation exposure of the inner ladders. For the legacy reprocessing, measurements were performed with higher granularity. Legacy measurements might have larger values compared to earlier reconstructions due to the higher granularity and because a decrease of the cluster position estimation error can result in an increase of the alignment position error. The values are zero, if the measurement accuracy is at least as good as the design values.

Uncertainties

Trends

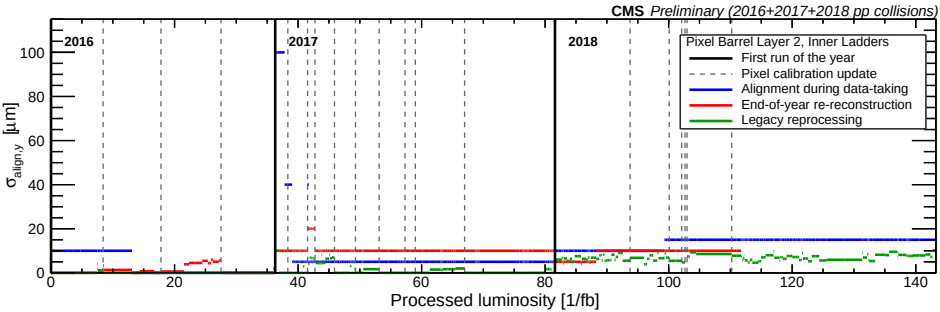

The contribution from the misalignment of the sensors to the total hit resolution for the inner ladders of the second pixel layer in local y-direction is shown for the Run 2 data-taking from 2016 to 2018 in dependency of the cumulative integrated luminosity. Shown are the results for the prompt reconstruction (blue), the end-of-year (EOY) re-reconstruction (red, notice there is no EOY re-reconstruction for the last $33\ \mathrm{fb}^{-1}$ of data-taking), and the legacy reprocessing (green). The vertical dashed lines indicate updates of the pixel calibration. The alignment error mainly varies between 0 and 20 mum and is only larger for the prompt-reconstruction in the beginning of the data-taking period in 2017, because the inner component (pixel detector) of the CMS tracking detector was replaced. The resolution of the second layer is better compared to the first layer due to the higher radiation exposure of the first layer. For the legacy reprocessing, measurements were performed with higher granularity. Legacy measurements might have larger values compared to earlier reconstructions due to the higher granularity and because a decrease of the cluster position estimation error can result in an increase of the alignment position error. The values are zero, if the measurement accuracy is at least as good as the design values.

Uncertainties

Trends

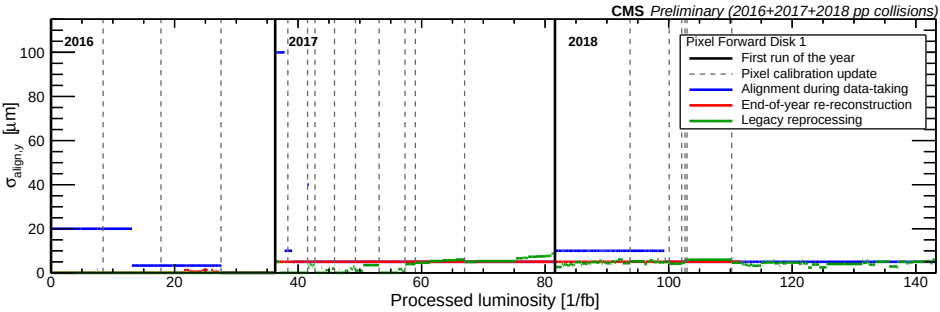

The contribution from the misalignment of the sensors to the total hit resolution for the first forward disk in the FPIX detector in local y-direction is shown for the Run 2 data-taking from 2016 to 2018 in dependency of the cumulative integrated luminosity. Shown are the results for the prompt reconstruction (blue), the end-of-year (EOY) re-reconstruction (red, notice there is no EOY re-reconstruction for the last $33\ \mathrm{fb}^{-1}$ of data-taking), and the legacy reprocessing (green). The vertical dashed lines indicate updates of the pixel calibration. The alignment error mainly varies between 0 and 20 mum and is only larger for the prompt-reconstruction in the beginning of the data-taking period in 2017, because the inner component (pixel detector) of the CMS tracking detector was replaced. For the legacy reprocessing, measurements were performed with higher granularity. Legacy measurements might have larger values compared to earlier reconstructions due to the higher granularity and because a decrease of the cluster position estimation error can result in an increase of the alignment position error. The values are zero, if the measurement accuracy is at least as good as the design values.

PCL

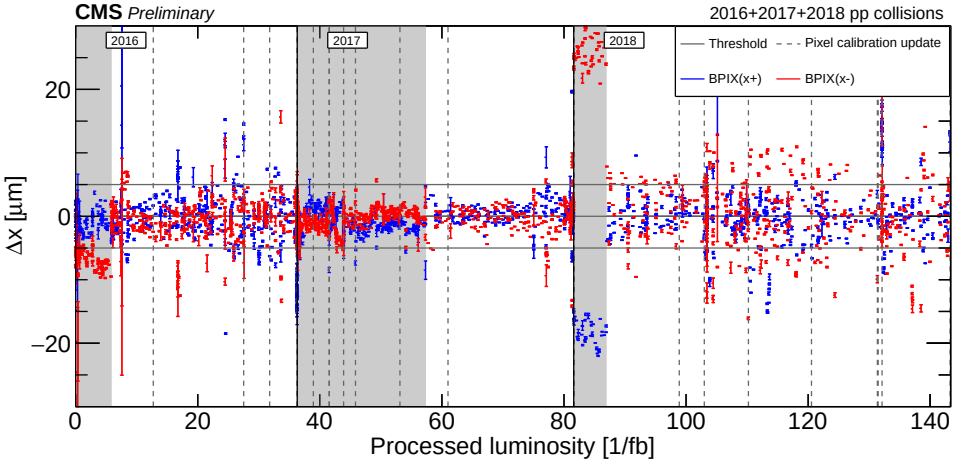

Observed movements in x direction of the two BPIX half-cylinders as a function of processed luminosity from the prompt calibration loop. Error bars represent the statistical uncertainties of the measurement. The vertical black solid lines indicate the first processed run for 2016, 2017, and 2018 data-taking period, respectively. Vertical dashed lines illustrate updates of the pixel calibration. The two horizontal lines show the threshold for a new alignment to be triggered. The grey bands at the beginning of each year indicate runs, where the automated updates of the alignment were not active. Missing points, especially at the beginning of 2018, correspond to periods where the automated alignment was not fully functional.

PCL

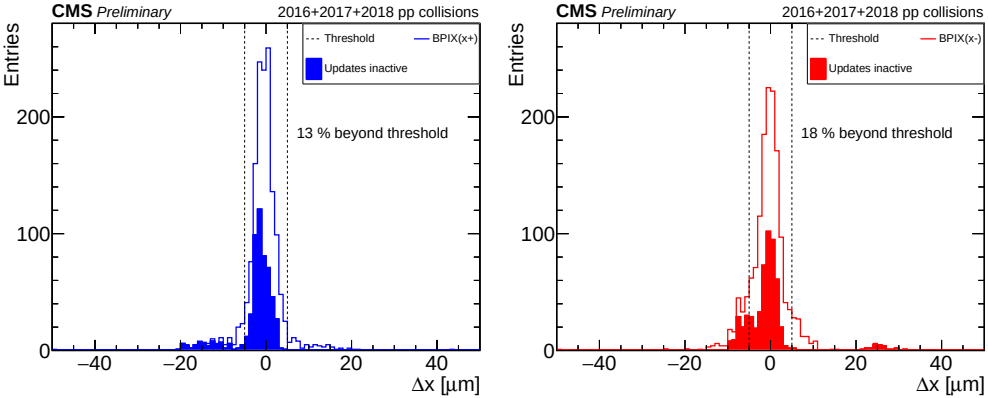

Observed movements in x direction of the two BPIX half-cylinders from the prompt calibration loop. The two vertical lines show the threshold for a new alignment to be triggered. The filled entries (Updates inactive) correspond to runs in early 2016, 2017, and 2018, where the automated updates of the alignment were not active. For both half-cylinders the fraction of runs, where a new alignment was triggered by the movement in x direction, is displayed. In this fraction the filled entries are not taken into account

CRUZET21

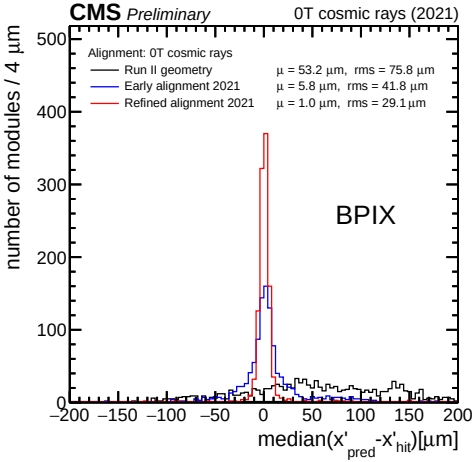

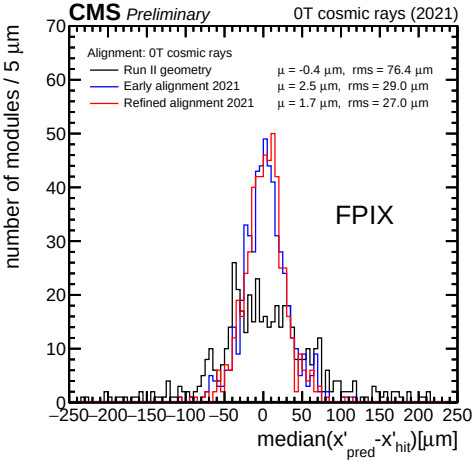

The following four figures show the distribution of median residuals in BPIX and FPIX modules, along the local-y (y') direction. Such residuals are computed by taking the difference between the measured hit position and the one predicted from the track fit. The distributions are obtained by refitting a set of approximately one million cosmic ray tracks recorded at 0 T with the alignment constants under consideration. For the refined alignment, the set of tracks used to build the distribution of median residuals has also been used to derive the alignment itself. After each alignment iteration, the mean of the distribution is closer to zero, and its width is reduced. The values shown in the plots are calculated considered the whole set of tracks, and are therefore sensitive to outliers with large residuals. The latter can originate from modules in the first layer, for which a measurement of the position relative to the ladder has not yet been performed, as well as from modules traversed by shallow tracks with consequently large clusters, for which the hit resolution is poor. The improvement of the refined alignment wrt. the early alignment is larger in BPIX than in FPIX, as the granularity of the alignment is only increased in the BPIX.

CRUZET21

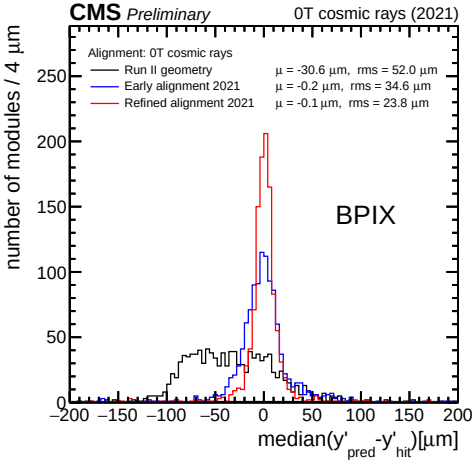

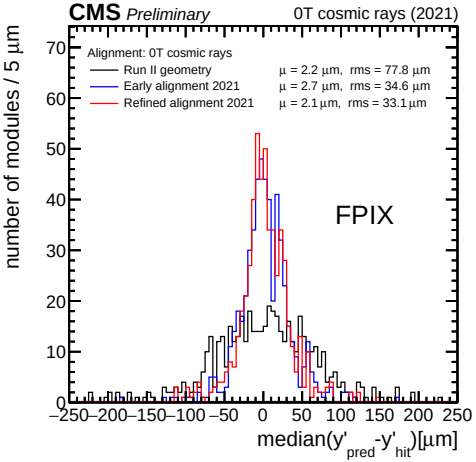

The following four figures show the distribution of median residuals in BPIX and FPIX modules, along the local-x (x') direction. Such residuals are computed by taking the difference between the measured hit position and the one predicted from the track fit. The distributions are obtained by refitting a set of approximately one million cosmic ray tracks recorded at 0 T with the alignment constants under consideration. For the refined alignment, the set of tracks used to build the distribution of median residuals has also been used to derive the alignment itself. After each alignment iteration, the mean of the distribution is closer to zero, and its width is reduced. The values shown in the plots are calculated considered the whole set of tracks, and are therefore sensitive to outliers with large residuals. The latter can originate from modules in the first layer, for which a measurement of the position relative to the ladder has not yet been performed, as well as from modules traversed by shallow tracks with consequently large clusters, for which the hit resolution is poor. The improvement of the refined alignment wrt. the early alignment is larger in BPIX than in FPIX, as the granularity of the alignment is only increased in the BPIX.

CRUZET21

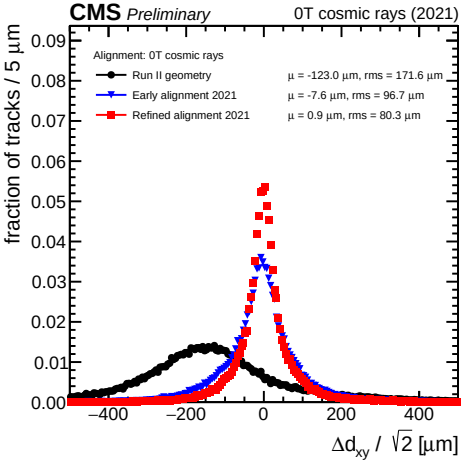

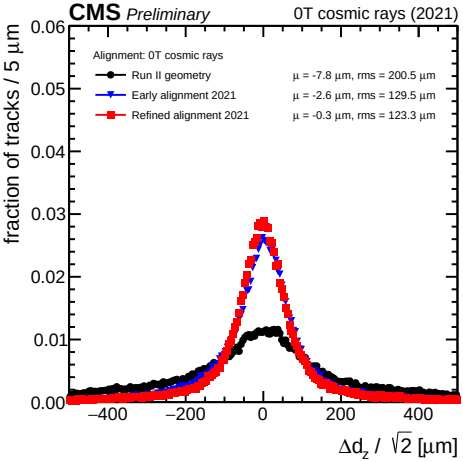

In the next two figures we show the difference in the track impact parameters in the transverse plane (d_{xy}) and in the longitudinal direction (d_z), when cosmic ray tracks passing through the pixel detector are split into two halves at the point of closest approach to the interaction region. The two half-tracks are refitted separately using the alignment constants under consideration. The width of the distributions measures the achieved alignment precision, while deviations of the mean from zero indicate possible biases. Such values are computed using the tracks in the plotted histogram range. An improvement is visible after each alignment iteration.

Acronyms I

BPIX Barrel Pixel. 3–5, 27, 34–38, 40–42, 59, 74, 75, 92, 93, 112–115

FPIX Forward Pixel. 3–5, 27, 40–42, 71, 76, 111, 114, 115

TEC Tracker End-Caps. 3–5

TIB Tracker Inner Barrel. 3–5

TID Tracker Inner Disk. 3–5

TOB Tracker Outer Barrel. 3–5

APE Alignment Parameter Errors. 57, 104

CMS Compact Muon Solenoid. 6–9

CRAFT Cosmic Run At Four Tesla. 43, 44

CRUZET Cosmic RUn at ZEro Tesla. 40–42

DMR Distribution of the Medians of the Residuals. 25, 26, 31–33, 57

DRNR Distribution of the RMS of the Normalised Residuals. 57

EOY End Of the Year. 60–65, 67–70, 73–75, 77–82, 84–93, 96–103, 105–111

GPU Graphics Process Unit. 56

HLS High-Level Structure. 19–21, 23, 24, 43, 44

IOV Interval Of Validity. 57

IP interaction point. 31–33

LHC Large Hadron Collider. 60–65, 77–82, 89–91, 100–103

ML Module Level (actually sensor level). 23–26

MTS Muon Track Split. 23, 24, 57

PCL Prompt-Calibration Loop. 77–79

PV Primary Vertex. 31–33, 57

ROC Read-Out Chip. 50

TBM Token-Bit Manager. 50

WM Weak Mode. 11–18

References I

The CMS Collaboration. **CMS Tracker Detector Performance**. https://twiki.cern.ch/twiki/bin/view/CMSPublic/DPGResultsTRK. Last modification: 2020-07-13.

Volker Blobel and Claus Kleinwort. "A New Method for the High-Precision Alignment of Track Detectors". In: **Proceedings of the Conference on Adcanced Statistical Techniques in Particle Physics** (2002).

Gianluca Cerminara and Broen Toon L Van Besien. **Automated workflows for critical time-dependent calibrations at the CMS experiment.** Tech. rep. CMS-CR-2015-091. 7. Geneva: CERN, May 2015. DOI: 10.1088/1742-6596/664/7/072009. URL: https://cds.cern.ch/record/2121263.

Sou-Cheng T Choi, Christopher C Paige, and Michael A Saunders. "MINRES-QLP: A Krylov subspace method for indefinite or singular symmetric systems". In: **SIAM Journal on Scientific Computing** 33.4 (2011), pp. 1810–1836.

Patrick L.S. Connor

patrick.connor@desy.de
Universität Hamburg
https://www.desy.de/~connorpa

MIN-Fakultät
Institut für Experimentalphysik
Tel.: +49 40 8998-2617
Geb.: DESY Campus 68/121

Center for Data Computing and natural Sciences
Tel.: +49 42838-6109
Geb.: Notkestraße 9